Ph.D. degree, Genomic and Experimental medicine

Scuola superiore meridionale (SSM),

University of Naples "Federico II"

Settore disciplinare: MED/03

Impaired nuclear glycogen metabolism affects liver homeostasis in argininosuccinic aciduria

Alfonso M. D'Alessio

TIGEM, Pozzuoli

Matricola DR99402

Supervisor: Prof. Nicola Brunetti-Pierri, Department of Translational Medicine, University of Naples "Federico II", TIGEM

Anno accademico 2023/2024

Table of contents

ABSTRACT

Urea cycle is the most important biochemical pathway for ammonia detoxification in humans. It takes place in mitochondria and cytoplasm of hepatocytes and incorporates ammonia derived from protein catabolism into urea, which is then eliminated in urine. Deficiencies of any of the enzymes involved in this pathway are responsible for rare inborn errors of metabolism known as urea cycle disorders (UCDs). Nuclear glycogen catabolism supports histone acetylation and reduced nuclear glycogenolysis drives progression of lung cancer through epigenetic changes. We found increased hepatic nuclear glycogen storage in $Asl^{Neo/Neo}$ mice, a mouse model of Argininosuccinic Aciduria (ASA), the second most common among UCDs. Notably, nuclear glycogen storage was detected in liver biopsies from ASA patients. Increased nuclear glycogen storage was associated with reduced nuclear abundance of glycogen phosphorylase (PYGL), the first and rate-limiting enzyme of glycogenolysis, suggesting impaired nuclear glycogenolysis. Nuclear glycogen storage was associated to marked decrease in lysine acetylation of several histones and histone 3, lysine 9 (H3K9)-dependent transcriptomic changes in $Asl^{Neo/Neo}$ mice. Treatment with a histone deacetylase inhibitor (HDACi) or adeno-associated viral vector (AAV) mediated gene transfer of *PYGL* in livers of $Asl^{Neo/Neo}$ mice improved survival and increased histone acetylation. Liver transcriptomic changes in $Asl^{Neo/Neo}$ mice highlighted dysregulation of metabolism, particularly lipid metabolism, including the master regulator of lipogenesis *Pparg* and the fatty acid receptor *Cd36*, that were restored in AAV-PYGL injected mice. Interestingly, I found increased nuclear glycogen storage and reduced nuclear PYGL histone acetylation in livers of a diet-induced rat model of metabolic dysfunction-associated fatty liver disease (MAFLD). ASL deficiency in both humans and mice leads to reduced Nitric oxide (NO) synthesis and treatment with NO donors restored nuclear PYGL in livers of $Asl^{Neo/Neo}$ mice. In summary, we propose that in ASA livers, impairment of NO-dependent nuclear translocation of glycogen metabolizing enzyme results in reduced glycogenolysis, nuclear glycogen storage and histone hypoacetylation that affect expression of lipid metabolism genes. Our findings have implications for the development of improved therapies for liver disease in ASA, but also common diseases such as MAFLD.

List of abbreviations

AAV: Adeno-associated viral vector
AGL: Glycogen branching enzyme
Agl: Murine glycogen branching enzyme gene
AMP: Adenosine mono-phosphate
AMPA: α-amino-3-hydroxy-5-methyl-4-i soxazolepropionic acid
AMPK: AMP activated kinase
ANOVA: Analysis of variance
ASA: Argininosuccinic aciduria
ASL: Human arginonosuccinate lyase gene
ASL: Argininosuccinate lyase
Asl: Murine argininosuccinate lyase gene
ASS1: Argininosuccinate synthetase 1
ATP: Adenosine tri-phosphate
cAMP: Cyclic AMP
CAT1: Cationic amino acid transporter 1
Cd36: Murine fatty acid translocase gene
cDNA: Complementary DNA
CNS: Central nervous system
CPS1: Carbamoyl phosphate synthetase 1
$CsCl_2$: Cesium chloride
DAPI: 4′,6-diamidino-2-phenylindole
DEG: Differentially expressed gene
DHAP/GAP: dihydroxyacetone-phosphate/glyceraldehyde-3-phosphate
DNA: Deoxyribonucleic acid
EDTA: Ethylenediaminetetraacetic acid
EGTA: Egtazic acid
ENCODE: Encyclopedia of DNA elements
FDR: False discovery ratio
G6P: Glucose-6-phosphate
GAA: Acid maltase
Gaa: Murine acid maltase gene
GAPDH: Glyceraldehyde 3-phosphate dehydrogenase
GC: Genome copies
GDE: Glycogen debranching enzyme
GDH: Glutamate dehydrogenase
GFP: Green fluorescent protein
GS: Glutamine synthetase
GSDs: Glycogen storage diseases
GSK3β: Glycogen synthase kinase 3 beta
GYS1: Glycogen synthase, isoform 1
GYS2: Glycogen synthase, isoform 2
H&E: Hematoxylin and eosin
H3K9: Histone 3, lysine 9
H3K9Ac: Acetylated lysine 9 of histone H3
H4K12Ac: Acetylated lysine 12 of histone H4
H4K5Ac: Acetylated lysine 5 of histone H4
HAT: Histone acetyltransferase
HCl: Hydrochloric acid
HDAC: Histone deacetylase
HDACi: HDAC inhibitor
HDL: High density lipoprotein
HFC: High fat, high cholesterol diet
HRP: Horseradish peroxidase
HSP90: Heat shock protein 90
i.p.: Intra-peritoneal
i.v.: Intravenous
IgG: Immunoglobulin G
KCl: Potassium chloride
KEGG: Kyoto encyclopedia of genes and genomes
LC3B: Microtubule-associated protein 1 light chain 3 beta
L-G6pc: Murine glucose-6-phosphatase alpha gene

LogFC: Logarithmic fold change
MAFLD: Metabolic dysfunction-associated fatty liver disease
$MgCl_2$: Magnesium chloride
mRNA: Messenger ribonucleic acid
NaCl: Sodium chloride
NADH: Reduced Nicotinamide adenine dinucleotide
NAFLD: Non-alcoholic fatty liver disease
NAG: N-acetyl glutamate
NH_3: Ammonia
NH_4^+: Ammonia ion
NO: Nitric oxide
NOS: Nitric oxide synthase
Ns: Non statistically significant
P62: Ubiquitin-binding protein p62
PAS: Periodic acid – Schiff
PBS: Phosphate-buffered saline
PC: Peri-central
PCR: Polymerase chain reaction
PFA: Paraformaldehyde
P-GYS2: Phosphorylated GYS2
PP: Peri-portal
Pparg: Murine peroxisome proliferator activated receptor gamma gene
PVDF: polyvinylidene difluoride
PYGB: Glycogen phosphorylase, brain isoform
PYGL: Glycogen phosphorylase, liver isoform
PYGM: Glycogen phosphorylase, muscle isoform
RNA: Ribonucleic acid
RT-PCR: Reverse transcriptase PCR
SAHA: Suberoylanilide Hydroxamic Acid, a.k.a. Vorinostat
SDS: Sodium dodecyl sulphate
SDS-PAGE: Sodium dodecyl-sulfate polyacrylamide gel electrophoresis
SEM: Standard Error of Mean
-SH: Free thiol group
S-NO: S-nitrosylated sulphurs
SNO-PYGL: S-nitrosylated PYGL
ST: Standard therapy
TBS: Tris-buffered saline
UCDs: Urea cycle disorders
WT: Wild type

INTRODUCTION

Ammonia metabolism

Nitrogen is the most abundant component of the atmosphere, and it is fixed into ammonia (NH_3) by nitrogen-fixing bacteria and archaea (Kuypers *et al.*, 2016). Ammonia dissolves in water as ionized form (ammonium, NH_4^+), that can be incorporated into amino acids and other nitrogen-containing species (Stein and Klotz, 2016). At physiological pH ammonia is largely in its ionized form. The concentration of ammonia in normal human plasma is 11-50 µmol/L (Brassant *et al.*, 2013). In humans, ammonia is constantly produced during the catabolism of nucleotides (purine and pyrimidine derivates), polyamines, and amino acids (Coomes, 2006). The liver is the primary organ involved in nitrogen homeostasis, which is maintained through two main metabolic pathways, glutamine synthesis and urea cycle, that are both necessary for ammonia detoxification (Haussinger, 1990). The two processes are zonated in the liver: while ureagenesis occurs in periportal hepatocytes, glutamine synthesis is restricted to pericentral ones (Cunningham and Porat-Shliom, 2021) (**Figure 1**). The brain cannot metabolize ammonia in normal condition, but upon hyperammonemia it can accumulate this metabolite into astrocytes, that in turns incorporate it into glutamine or alanine (Wilkinson *et al.*, 2010).

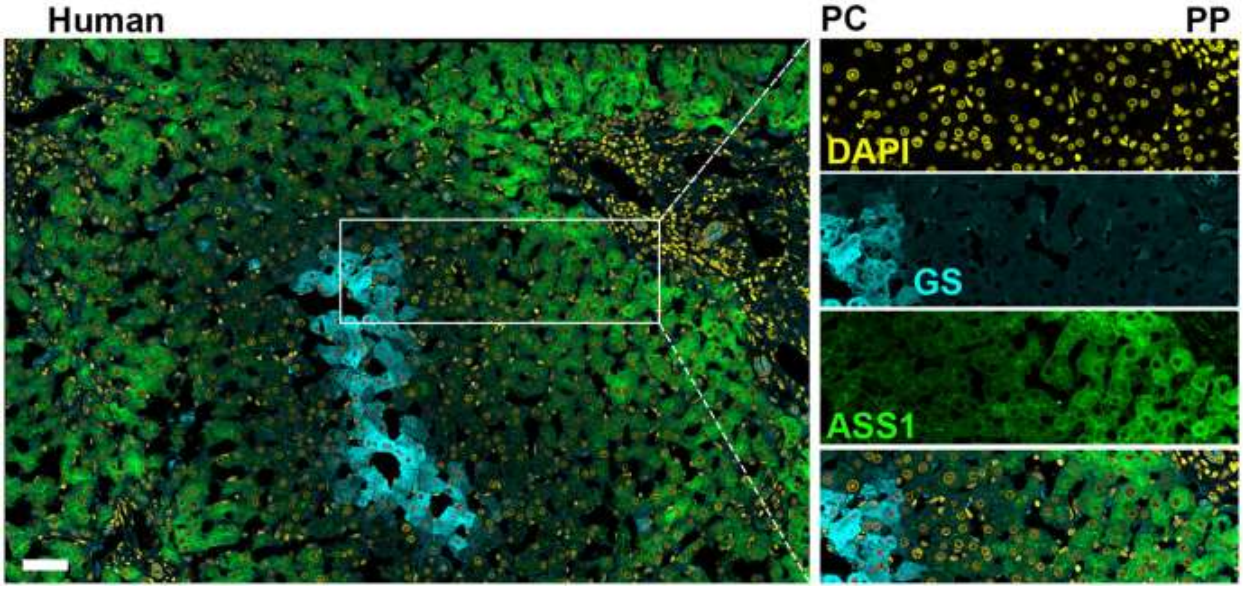

Fig. 1. Human liver with pericentral (PC) hepatocytes stained for argininosuccinate synthase 1 (ASS1, one of the enzymes of the urea cycle, green) and periportal (PP) hepatocytes stained for glutamine synthase). Nuclei are stained in DAPI (yellow). Scale bar = 50 µm. Adapted from (Cunningham and Porat-Shliom, 2021).

The urea cycle is a low-affinity, high-capacity pathway in periportal hepatocytes and is the main pathway for ammonia detoxification in *Homo sapiens* and other ureotelic animals. The urea cycle is made by six enzymes and two transporters, that catalyze a series of reactions taking place in both mitochondria and cytosol. The conversion from ammonia to urea involves five catalytic enzymes (carbamoyl phosphate synthetase I, ornithine transcarbamylase, argininosuccinate synthase, argininosuccinate lyase, and arginase), plus one enzyme that synthesizes an allosteric activator of carbamoyl phosphate synthetase I (N-acetylglutamate synthase) (**Figure 2**). Arginine – one of the intermediates of the urea cycle – is used as a substrate by nitric oxide synthase (NOS) for the synthesis of nitric oxide (NO) (Alderton *et al.*, 2001). NO is a key regulator of vascular smooth muscle compliance, and defects in its production are relevant for a large number of diseases mainly hypertension and

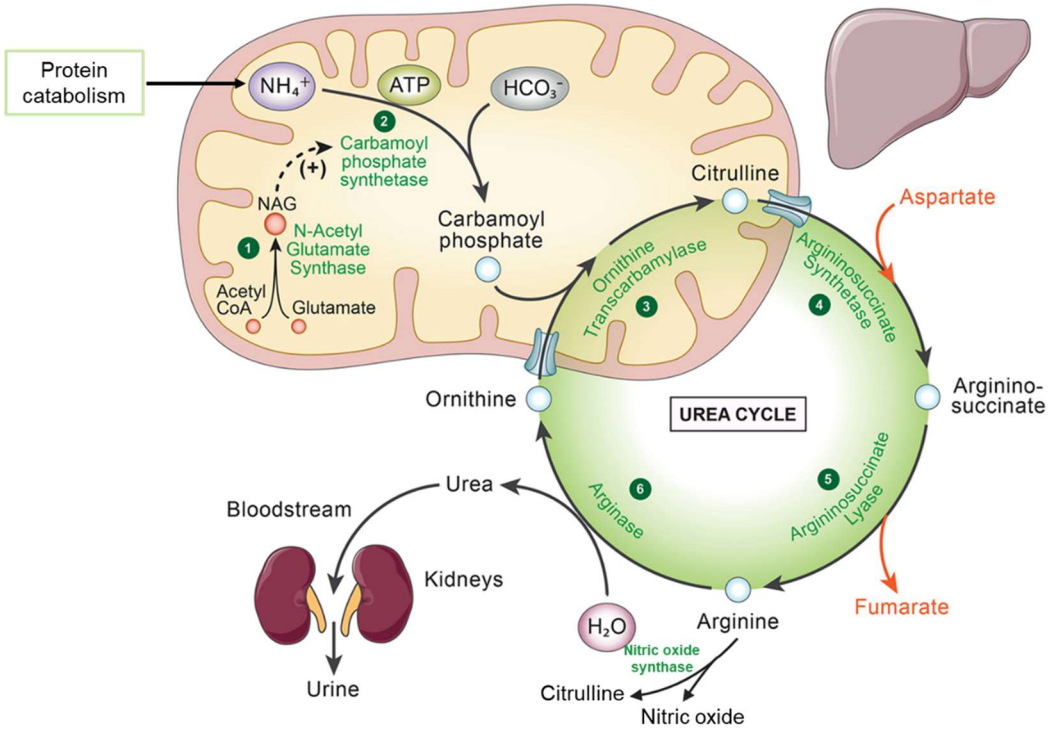

Fig. 2. Schematic representation of the urea cycle. The urea cycle converts ammonia into urea that is excreted by the kidneys in the urine. Urea is formed from ammonia, bicarbonate, aspartate-derived nitrogen and ATP. The incorporation of ammonia into urea requires five enzymatic steps. The first and rate-limiting reaction is the synthesis of carbamoyl phosphate by carbamoyl phosphate synthetase I (CPS1) that is allosterically regulated by the presence of N-acetylglutamic acid (NAG). Adapted from (Nitzahn and Lipshutz, 2020).

cerebrovascular disease (Chaklaki *et al.,* 2020; Wang *et al.*, 2022). NO is also the substrate for post-translational modification of proteins including tyrosine nitration and cysteine nitrosylation. Tyrosine nitration has been described in more than 900 proteins (Griswold-Prenner *et al.*, 2023) and occurs under oxidative stress conditions (He *et al.*, 2019; Jiang *et al.*, 2022; Rocha *et al.*,

2013). Cysteine nitrosylation has been found in more than 1,000 proteins (Doulias *et al.*, 2013; Gould *et al.*, 2013) and regulates several processes including protein stability, enzyme activity and intracellular location (Kumari *et al.*, 2022; Malik *et al.*, 2010; Wang *et al.*, 2018).

Hyperammonemia and urea cycle disorders

Hyperammonemia is defined as a concentration of ammonia in the blood higher than 50 µmol/L (> 75 µmol/L in term newborns) (Braissant *et al.*, 2013). Ammonia crosses the blood-brain barrier in its non-ionized form. Increased ammonia in the central nervous system (CNS) results in neurologic signs of brain damage including tremor, ataxia, drowsiness, seizures that can evolve in coma and death. The mechanisms underlying CNS damage during hyperammonemia are not completely understood yet. Upon hyperammonemia, ammonia is incorporated into glutamine in astrocytes, and the accumulation of intracellular glutamine in astrocytes is thought to be a major cause of brain damage, because glutamine is osmotically active and attracts water leading to astrocyte swelling (Brusilow *et al*., 2010). Hyperammonemia can also interfere with glutamatergic neurotransmission (Matsumoto *et al*., 2019). Acute hyperammonemia leads to excitotoxic cell death, accumulation of glutamate into the extracellular space, decreased brain glutamate and loss of α-amino-3-hydroxy-5-methyl-4-isoxazolepropionic acid (AMPA) receptors (Matsumoto *et al*., 2019).

Impaired ammonia hepatic detoxification results from a wide range of causes including non-genetic diseases (e.g., liver cirrhosis, acute liver failure, portosystemic shunting) (Häberle 2013) and genetic disorders. Deficiencies of any of the enzymes of the urea cycle, known as urea cycle disorders (UCDs), are a group of rare inherited metabolic disorders with an overall estimated incidence of 1 in 35,000 births (Ah Mew *et al*., 2003). UCDs are autosomal recessive disorders, with an exception being ornithine transcarbamylase deficiency, that is X-linked. The clinical severity of each disease depends on the position of the defective enzyme in the urea cycle with the most severe being CPS1 deficiency (CPS1 is the first enzyme of the pathway), and the degree of its reduced activity. Complete loss of functions of urea cycle enzymes typically have an onset at birth or in newborn period with severe hyperammonemia presenting with non-specific clinical signs and symptoms including failure to feed, hypothermia, drowsiness (Kolker *et al.*, 2015). A significant portion of neonates develop seizures. Hyperventilation secondary to cerebral edema is a common early finding and can cause respiratory alkalosis (Summar and Ah Mew, 2018). In

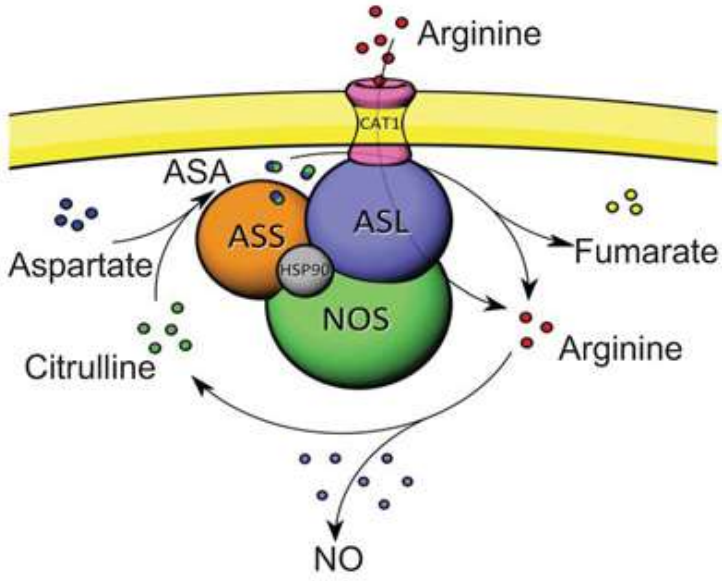

Fig. 3. Schematic representation of the multimeric complex formed by argininosuccinate lyase (ASL), argininosuccinate synthetase 1 (ASS), nitric oxide synthase (NOS) and the anionic amino acid transporter CAT1 together with the heat shock protein 90 (HSP90). This complex finely regulates arginine metabolism and NO synthesis. Adapted from (Erez *et al*., 2011).

milder (or partial) urea cycle enzyme deficiencies, the disease onset occurs later in life (Summar and Ah Mew, 2018). UCDs have poor outcomes especially in cases of misdiagnosis or delayed diagnosis (Brusilow, 1995).

Among the UCDs, argininosuccinic aciduria (ASA) is the second most common disease, accounting for 16% of all UCDs (Summar *et al.*, 2013). ASA is due to deficienct of argininosuccinate lyase enzyme (ASL) that converts argininosuccinate into arginine and fumarate in the cytosol of hepatocytes. The reaction catalyzed by ASL is also part of the citrulline-NO cycle, that generates NO from arginine through the NOS enzyme. ASL is a homotetrameric enzyme (Turner *et al.*, 1997), encoded by a highly conserved gene (Crosas *et al.*, 2015; O' Brien *et al.*, 1986; Sampaleanu *et al*., 2002). ASL is part of a multimeric complex together with the amino acid transporter CAT1, the urea cycle enzyme Argininosuccinate synthetase 1 (ASS1) and the NOS (Erez *et al.*, 2011). In this complex, ASL plays a double role both producing arginine and maintaining this multi-enzymatic complex that enhances NO synthesis (**Figure 3**).

ASA can present either with an early neonatal-onset hyperammonemia and a broad spectrum of manifestations including neurocognitive, gastrointestinal, hypokalemia, and liver manifestations (Kolker *et al.*, 2015; Nagamani *et al.*, 2012). About one half of ASA patients develop liver disease, with hepatomegaly or isolated transaminitis being the most common ones (Baruteau *et al*., 2017) but chronic impairment of the liver synthetic function (Marble *et al.*, 2008), liver fibrosis and cirrhosis (Marble *et al*., 2008), and hepatocellular carcinoma have been also reported (Baruteau *et al.*, 2017). Notably, the hepatopathy is unrelated to the increased blood ammonia (Mori *et al.*, 2002). Neurologic involvement occurs in more than 90% of ASA patients

(Baruteau *et al.*, 2017) with variable manifestations including developmental delay, intellectual disability (Baruteau *et al.*, 2019; Waisbren *et al.*, 2016), epilepsy (Elkhateeb *et al.*, 2023; Grioni *et al.*, 2011), ataxia, tremor, dystonia and myopathy-like symptoms (Baruteau *et al.*, 2017). Psychiatric manifestations include autism-like features, psychosis and even schizophrenia (Baruteau *et al.*, 2019). In contrast to proximal UCDs due to mitochondrial enzymes, neurological involvement in ASA is not strongly correlated to episodes of hyperammonemia (Baruteau *et al.*, 2019) and it has been proposed that brain damage may be a consequence of NO deficiency-dependent disruption of the blood-brain barrier (Kho *et al.*, 2023). Systemic blood hypertension (Brambilla *et al.*, 2019; Brunetti-Pierri *et al.*, 2009) has also been correlated to NO deficiency (Nagamani *et al.*, 2012). Untreated patients often show slower hair growth, alopecia and tricorrhexis nodosa (Coulter *et al.*, 1982) that usually resolve after arginine supplementation (Nagamani *et al*., 2012). ASA patients have also been found to have a lipid metabolism disorder with increased blood cholesterol and reduced HDL cholesterol (Brambilla *et al.*, 2019) and fatty changes in the liver (Yaplito-Lee *et al*., 2013).

Current therapy for ASA aims at correcting arginine deficiency and preventing hyperammonemia. Therefore, low-protein diet in combination with arginine and citrulline supplementations is used to reduce the risk of hyperammonemia (Häberle *et al.*, 2019). Because high doses of arginine have been associated with increased transaminases (Nagamani *et al.*, 2012), current recommendations are based on low-dose arginine together with ammonia scavengers (Häberle *et al.*, 2019). In a mouse model of ASA, the $Asl^{Neo/Neo}$ mice, NO supplementation has shown to significantly improve survival (Erez *et al.*, 2011). A single-patient trial found improved blood pressure and neurocognitive phenotype upon treatment with NO donors (Nagamani *et al.*, 2012) and two ongoing clinical trials are investigating the efficacy of NO donor at improving blood pressure and neurocognition in ASA patients (NCT02252770; NCT03064048). Liver transplantation has been performed for UCDs including ASA and it allows patients to discontinue low-protein diet and ammonia scavenges. However, liver transplantation does not revert pre-existing brain damage (Newnham *et al.*, 2008; Perito *et al.*, 2014). As safer and non-invasive alternative to liver transplantation, gene and mRNA therapies have been investigated in the $Asl^{Neo/Neo}$ mouse model (D'Alessio *et al.*, 2024). Overall, liver-directed gene-based therapies corrected the ureagenesis defect as shown by extended survival and biochemical correction (Ashley *et al.*, 2018) but had limited efficacy on the other systemic manifestations of ASA (Gurung

et al., 2024).

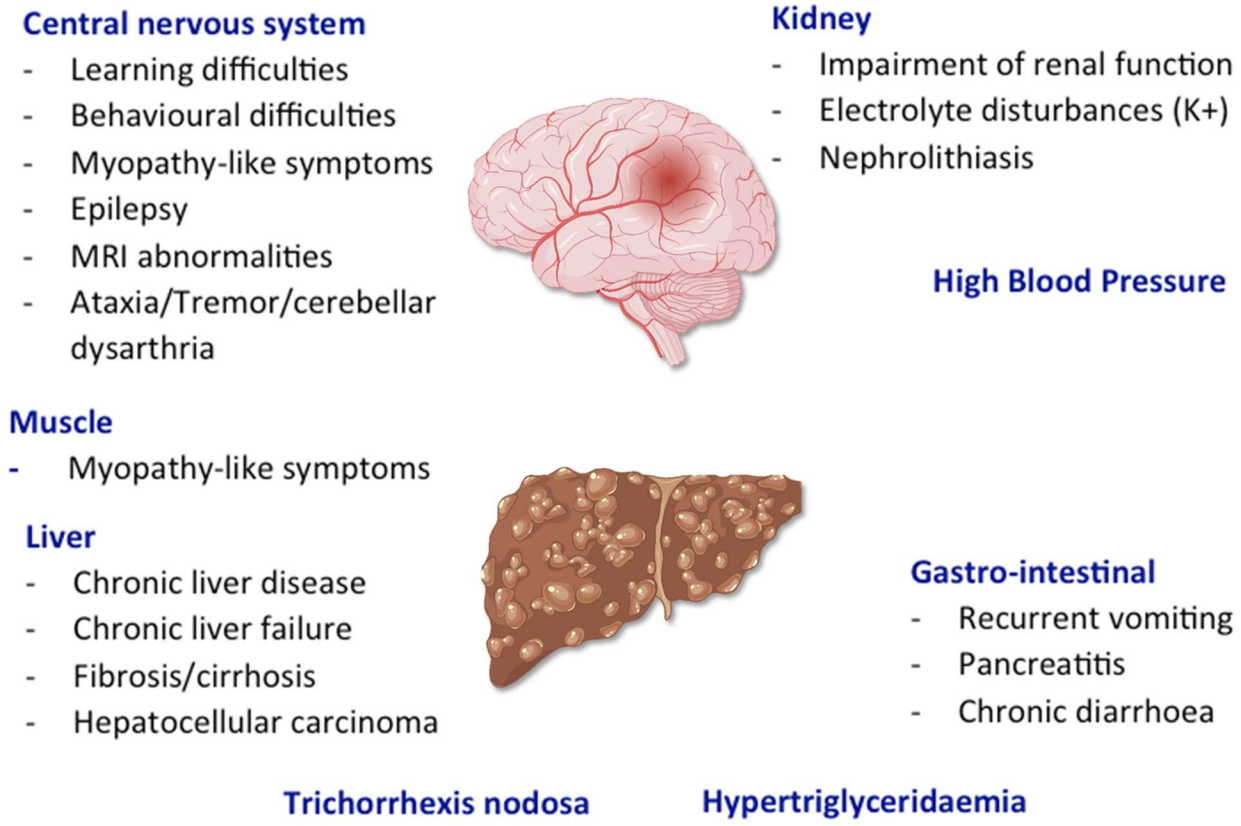

Fig. 4. Main clinical features of argininosuccinic aciduria (ASA). Compared to other UCDs, ASA affects several organs and tissues. Adapted from (Baruteau *et al.*, 2019).

Glycogen

Glycogen is a branched polymer of glucose playing an important role in energy homeostasis (Preiss and Walsh, 1981). Discovered in 1857 by Claude Bernard (Young, 1957), glycogen is present in the majority of living beings, from archaea and bacteria to *H. sapiens* (Roach *et al.*, 2012). In humans, glycogen is largely stored in liver and muscle. In liver glycogen is used to supply glucose in the blood upon fasting (Calder and Geddes, 1985). Muscle glycogen is used to provide energy for contraction.

Glycogen is a polymer made by glucose monomers combined into a branched chain by (1 → 4)-α or (1 → 6)-α covalent bonds. The (1 → 4)-α bonds join glucose molecules in a linear chain, whereas the (1 → 6)-α linkages introduce a tree-like branching pattern. This arrangement leads to the formation of the glycogen "β particles", 20 nm spherical structures detected under electron microscopy (Rybicka, 1996). In the liver, β particles combine to form more complex and larger

300 nm diameter structures known as α particles that display a "rosette" appearance (Liu and Gilbert, 2024). Glycogen is nonvisible with routine hematoxylin-eosin (H&E) staining, but it can be visualized by periodic acid-Schiff (PAS) staining. The specificity of the signal can be evaluated by the application of diastase (α-amylase) resulting in the disappearance of the PAS staining (Layton *et al.*, 2019).

Glycogen synthesis is coordinated by three enzymes: i) glycogenin, which primes the formation of a 8-12 monomers long glucose chain; ii) glycogen synthase (GYS), which is recruited at the C-terminus of glycogenin and interacts with the newly-formed chain to lengthen it through the addition of (1 → 4)-α glycosidic linkages, and iii) glycogen branching enzyme that generates (1 → 6)-α bounds every 6-8 residues adding branches to the growing polymer, thus creating its globular form (Marr *et al.*, 2022; Roach, 2002). Both glycogenin and GYS exist in two isoforms with differential expression in different tissues (Curtino and Aon, 2019; Palm *et al.*, 2013; von Wilamowitz-Moellendorff *et al.*, 2013). Isoform 1 of GYS (GYS1) is mainly expressed in skeletal muscle whereas the expression of isoform 2 of glycogen synthase (GYS2) is restricted to the liver (Nuttall *et al.*, 1994). GYS is the rate-limiting enzyme in glycogen synthesis, and its activity is activated allosterically by binding glucose-6-phosphate (G6P) (Baskaran *et al.*, 2010). Conversely, GYS phosphorylation at several residues has an inhibitory effect and is operated by several kinases, including glycogen synthase kinase 3β (GSK3 β) and 5'AMP-activated protein kinase (AMPK) (Andeva-Andany *et al.*, 2016). GYS phosphorylation is regulated by a positive feedback loop, in which phosphorylation of a specific residue acts as a recognition motif for phosphorylation of other residues (Marr *et al.*, 2022). Dephosphorylation of GYS by glycogen-associated phosphatases of type 1 (PP1) has an activating effect on it (Adeva-Andany *et al.*, 2016; McCorvie *et al.*, 2022).

Glycogenolysis is the degradation of glycogen into glucose monomers and it is carried out by two distinct pathways. The first pathway takes place in the cytosol and involves two enzymes, namely the glycogen phosphorylase and the glycogen debranching enzyme (GDE). Glycogen phosphorylase is the kinase responsible for detaching glucose-1-phosphate residues from glycogen linear chains, thus disrupting (1 → 4)-α glycosidic linkages. There are three tissue-specific isoforms of glycogen phosphorylase, namely PYGM (muscle), PYGB (brain), and PYGL (liver) (Adeva-Andany *et al.*, 2016; Burwinkel *et al.*, 1998). The activities of glycogen phosphorylases are controlled by allosteric regulators: G6P and UDP-glucose that inhibit their activities (Ercan-

Fang *et al.*, 2002). PYGM is activated by interaction with AMP and increased glycogen content in the muscle (Adeva-Andany *et al.*, 2016). In the liver, PYGL is positively regulated by glucagon in a cyclic-AMP (cAMP) dependent manner (Keppens *et al.*, 1993). The activity of glycogen phosphorylase is regulated by phosphorylation that promotes glycogenolysis (Semrau *et al.*, 2022) in response to increased calcium and cAMP (Bali *et al.*, 2014). However, glycogen phosphorylase cannot remove glucose 1-phosphate from the glycogen at the branching point and the activity glycogen debranching enzyme (AGL) is required to make the branching points accessible to the action of glycogen phosphorylase. AGL has indeed two catalytic activities, α-1,4-glucanotransferase and amylo-α-1,6-glucosidase. The second pathway of glycogen degradation occurs in the lysosomes (Koutsifeli *et al.*, 2022) where glycogen is hydrolyzed to glucose by the acid α-1,4-glucosidase, 1,4-α-glucan hydrolase or acid maltase (GAA) (Adeva-Andany *et al.*, 2016).

Glycogen storage diseases

Glycogen storage diseases (GSDs) are a group inherited metabolic disorders due to defects in glycogen synthesis and degradation (Hannah *et al.*, 2023) that almost invariably show abundant glycogen deposition in tissues, mostly muscle and liver (Ozen, 2007). Unexpectedly, some GSDs are due to deficiency of enzymes involved in glycogen synthesis, such as deficiency of muscle isoform of

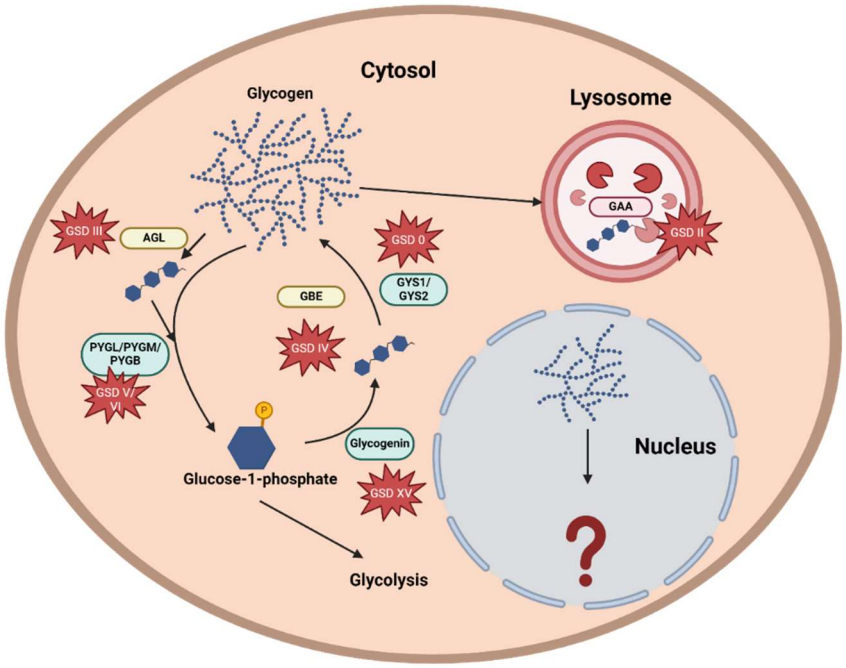

Fig. 5. Glycogen metabolism. Spiked balloons indicate enzymes deficient in glycogen storage diseases (GSD) associated with deficiency of each enzyme. PYGL/PYGM/PYGM, three different isoforms of glycogen phosphorylase; GBE, glycogen branching enzyme; GYS1/GYS2, two different isoforms of glycogen synthase; GAA, lysosomal acid glucosidase.

glycogenin that is responsible for GSD XV (Malfatti *et al.*, 2014), deficiency of GYS1 that is responsible for GSD type 0b, and deficiency of GYS2 that is responsible for GSD type 0a (Musumeci *et al.*, 2022). Deficiencies of PYGM, PYGL, AGL or GAA are all responsible for GSDs (**Figure 5**).

Glycogenated nuclei

In hepatocytes, most glycogen is located in the cytosol, with up to 10% located in the lysosomes (Roach, 2002). Glycogen inside the nuclei of hepatocytes, was first reported in the 19th century by Paul Ehrlich (Ehrlich, 1883). Glycogenated nuclei have been detected in several diseases including diabetes, fatty liver disease, Wilson disease and porphyria cutanea tarda (Fitzpatrick *et al.*, 2014; Lefkowitch and Grossman, 1983; Pronicki, 2017; Takahashi and Fukusato, 2014;). Glycogenated nuclei have been also reported as markers for hepatocyte senescence (Aravinthan *et al.*, 2012). Interestingly, while glycogenated nuclei are frequent (up to 75% of cells, **Table 1**) in non-alcoholic fatty liver disease (NAFLD), a condition that has been recently renamed as metabolic dysfunction-associated fatty liver disease (MAFLD) (Eslam *et al.*, 2020a; Eslam *et al.*, 2020b), but they are usually absent in alcoholic fatty liver disease and alcoholic steatohepatitis (Pinto *et al.*, 1996). Two types of nuclear glycogen inclusions have been described: type 1 nuclear inclusions including glycogen associated with autophagy- and lysosome-related proteins (LC3B, p62, Cathepsin B) within a membrane bordered structure, and type 2 nuclear inclusions that are devoid of membrane and exclusively made of glycogen

Author, year	Number of biopsies	Steatosis (%)	Glycogenated nuclei (%)
Adler, 1979	29	100	41
Itoh, 1987	17	100	76
Nagore, 1988	9	100	100
Lee, 1989	49	100	35
Bacon, 1994	33	100	97
Baldridge, 1995	15	100	100
Pinto, 1996	32	100	75
Brunt, 1999	51	100	86

Table 1. Percentage of glycogenated nuclei in the liver of patients suffering from non-alcoholic fatty liver disease. Adapted from (Brunt, 2001).

(Schwertheim *et al.*, 2020) (**Figure 6**). Glycogen storage in the liver is observed in UCDs (Bigot *et al.*, 2017) and it has been thought to be related to amino acid supplementation (Bigot *et al.*, 2017). Few reports reported glycogen in the cytosol of hepatocytes patients and mice with ASA (Bigot *et al.*, 2017; Burrage *et al.*, 2020; Yaplito-Lee *et al.*, 2013). Moreover, our group observed glycogen storage not only in the cytosol but also in the nuclei of hepatocytes of ASA mice (Soria *et al.*, 2021) (**Figure 7**). However, to date, the role of nuclear glycogen is still elusive. Nevertheless, it was shown that glycogen can be synthesized *de novo* in the nuclei of cells, without exchanges between the nuclear and cytosolic glycogen pools (Sun *et al.*, 2019). Nuclear glycogen is used for *in situ* production of glucose, that is metabolized through a nucleus-based glycolytic pathway for the synthesis of acetyl-CoA required for histone acetylation regulating gene expression (Boukouris *et al.*, 2016; Sun *et al.*, 2019).

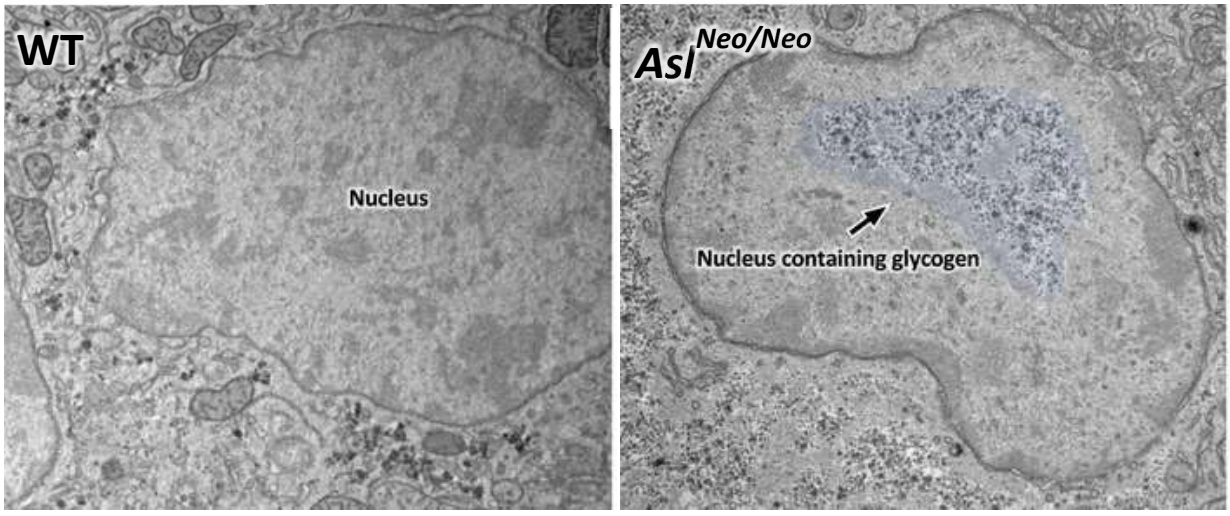

Fig. 7: Electron microscopy images show liver glycogen deposition in the nuclei of *Asl*$^{Neo/Neo}$ mice, but not in WT ones. Adapted from (Soria *et al.*, 2021).

AIM OF THE THESIS

Our group recently found that livers of the *Asl*$^{Neo/Neo}$ mice, a mouse model of ASA, have nuclear glycogen storage (Soria *et al.*, 2021). Nuclear glycogen has been reported in livers of various diseases and in cancer cells, nuclear glycogen storage drives cancer progression through reduced glycogenolysis, histone hypo-acetylation and transcriptomic changes (Sun *et al.*, 2019).

The goal of this thesis work was to investigate the mechanisms underlying nuclear glycogen storage in ASA livers, and its consequences on liver homeostasis.

MATERIALS AND METHODS

Human samples

The study was conducted according to the guidelines established in the Declaration of Helsinki. Frozen liver samples from patients affected from ASA who received liver transplantation were obtained from Ospedale Pediatrico Bambino Gesù (Rome, Italy). Liver samples from patients who received liver transplantation for other unrelated reasons were used as controls. The study received approval by the ethics committee of Ospedale Pediatrico Bambino Gesù.

Animal studies

All mouse procedures were performed in accordance with regulations and were authorized by the Italian Ministry of Health. *Asl*$^{Neo/Neo}$ mice (B6.129S7-*Asl*^{tm1Brle}/J) were purchased from Jackson Laboratory (Bar Harbor, ME, USA) and housed in ventilated cages in a 12-h light-dark cycle environment. Animals were inbred and maintained on standard rodent chow (Harlan 2018, Teklab Diets, Madison, WI, USA; protein content 18%) with water *ad libitum*. Mouse genotyping with DNA extracted from finger clips was performed as previously reported (Erez *et al.*, 2011). Two different PCR reverse primers, paired with the same forward one, were used to discriminate wild type (WT) and recombinant alleles of *Asl* gene. Both female and male mice were used for experiments. *Asl*$^{Neo/Neo}$ mice body weight was evaluated daily from 10 days of age. For all long-term experiments, all WT and *Asl*$^{Neo/Neo}$ mice received a supportive treatment modified (Baruteau *et al.*, 2018) consisting in daily intra-peritoneal (i.p.) injections of sodium benzoate (0.5 g/kg/day) and L-Arginine (0.5 g/kg/day) from day 10 to day 30. For sodium nitrite experiment, *Asl*$^{Neo/Neo}$ mice received daily i.p. injections of sodium nitrite (10 mg/kg) from 10 days of age to the age of euthanasia. For vorinostat (SAHA) treatment, *Asl*$^{Neo/Neo}$ mice received i.p injections of SAHA (50 mg/kg) three times per week, from day 10 to day 30. Concomitantly, all these mice received daily supportive treatment to improve survival until day 30. WT littermates were used as controls. For all experiments, WT and *Asl*$^{Neo/Neo}$ littermates were housed in the same cages. Pups and their mothers were fed with the same diet. Blood samples for biochemical measurements were collected by retro-orbital bleedings. Treated animals were sacrificed by cervical dislocation at indicated time points; liver, skeletal muscle, and brain were harvested for analysis. The efficacy of Myc-tagged human *PYGL* gene transfer was assessed in WT mice through intravenous (i.v.) injection in the retro-orbital plexus of a dose of $1x10^{13}$ genome copies (GC)/kg of the AAV-PYGL. Mice were

sacrificed 4 weeks after injection and livers were harvested. For *PYGL* gene transfer in *Asl*$^{Neo/Neo}$ mice, 7 days old *Asl*$^{Neo/Neo}$ mice received a single i.v. injection in the retro-orbital plexus of a dose of $1x10^{13}$ genome copies (GC)/kg of the AAV-PYGL vector. Mice were sacrificed at 30 days of age and protein expression was evaluated by western blotting on liver lysates.

Liver samples of *Ass1*^{Fold} mice, a hypomorphic mouse model of Argininosuccinate synthetase 1 deficiency (Lisjak *et al.*, 2023), and of *spf-ash* mice, a mouse model of ornithine transcarbamylase deficiency (Soria *et al.*, 2021) were obtained from from International Centre for Genetic Engineering and Biotechnology (ICGEB, Trieste, Italy). Liver samples of mice with liver-specific deficiency of Argininosuccinate synthetase 1 (*Ass1* LiKO; Keshet *et al.*, 2020) were obtained from Weizmann Institute of Science (Revohot, Israel). Liver samples of *Gaa*$^{-/-}$ mice, a murine model of acid maltase deficiency (glycogen storage disease II; Tarallo *et al.*, 2021) were obtained from Department of Translational medicine, University "Federico II" (Naples, Italy). Liver samples of *Agl*$^{-/-}$ mice, a mouse model of glycogen debranching enzyme deficiency (GSD III; Vidal *et al.*, 2018) and of *L-G6pc*$^{-/-}$ mice, a mouse model of glucose-6-phosphatase deficiency (GSD Ia; Mutel *et al.*, 2011) were obtained from Institut national de la santé et de la recherche médicale (INSERM; Evry, France). Liver samples of *Pygl*$^{-/-}$ mice, a mouse model of PYGL deficiency (GSD VI; Wilson *et al.*, 2019) were obtained from Department of Pediatrics, University of Connecticut (Farmington, CT, USA). Liver samples of rats treated with a high fat, high cholesterol (HFC) diet for two weeks, a model of mild MAFLD (Thomsen *et al.*, 2014) were obtained from Department of Clinical medicine, hepatology and gastroenterology, University of Aarhus (Denmark).

Electron microscopy

Frozen liver specimens were fixed in 1% glutaraldehyde in 0.2 M HEPES buffer. Small fragments of them were then post-fixed in OsO4 and uranyl acetate. Samples were dehydrated through a series of ethanol solutions and propylene oxide and then embedded in epoxy resin and polymerized for 72 h at 60 °C. Thin sections of each sample were cut with a Leica EM UC7 ultramicrotome. Image acquisition was performed using an FEI Tecnai – 12 electron microscope (FEI, Eindhoven, The Netherlands) equipped with Veletta CCD camera (Olympus, Lakewood, CO, USA) for digital image acquisition.

Generation of adeno-associated viral vectors (AAVs)

The human *PYGL* cDNA was purchased by OriGene Technologies Inc. (Rockville, MD, USA) and subcloned into a pAAV2/8.TBG.GFP plasmid (Auricchio *et al.*, 2001). GFP was removed by enzyme digestion using NotI and HindIII. Myc-tag was inserted in frame in the same vector for transgene expression control. AAV vectors were produced by Innovavector s.r.l. (Pozzuoli, Italy) by triple transfection in HEK293 cells and purified by $CsCl_2$ ultracentrifugation. Physical titers of viral vector preparations, expressed as genome copies/ml, were determined by real-time PCR quantification using TaqMan (Applied Biosystems, Foster City, CA) and dot-blot analysis as previously described (Doria *et al.*, 2013). Average values between PCR quantification and dot-blot results were used to calculate the final titer of each prep.

Cell lysis, subcellular fractionation and Western blot analysis

For subcellular fractionation, 10 mg of liver samples were suspended in cytosol isolation buffer (250 mM sucrose, 20 mM HEPES, 10 mM KCl, 1.5 mM $MgCl_2$, 1 mM EDTA, 1 mM EGTA, pH 7.4) supplemented with protease and phosphatase inhibitor cocktails (Complete and PhosSTOP Roche, Roche Diagnostics, Basel, Switzerland) and homogenized on ice using a Teflon pestle and mortar. Lysates were subsequently centrifuged at 1000 × *g* for 10 min at 4 °C to pellet the nuclei while cytosolic fractions remained in the supernatant. Nuclei-containing pellets were washed with PBS twice; after every wash, samples were centrifuged at 800 × *g* for 10 min at 4 °C. Pellets containing nuclei were then re-suspended in nuclear lysis buffer (0.5 M NaCl , 20mM HEPES, 1.5 mM $MgCl_2$, 0.2 mM EDTA, 20% glycerol, 1% Triton X-100) supplemented with protease and phosphatase inhibitor cocktails and incubated on ice for 30 min, during which they were vortexed three times, and then sonicated three times at 3 Å for ~10 s. Samples were then centrifuged for 15 min at 16,000 × *g*. The supernatant contained the enriched nuclear fraction. The same protocol was used for subcellular fractionation of skeletal muscle and brain tissue. For whole cell lysates, liver samples were suspended in Radio-Immunoprecipitation assay (RIPA) buffer (50 mM TRIS-HCl, 0,15 M NaCl, 1mM EDTA, 1% Triton X-100, 0,1% SDS, pH 7.4) supplemented with protease and phosphatase inhibitor cocktails and homogenized with stain beads using TissueLyser LT (Qiagen, Hilden, Germany) for 3 minutes at 30 Hz. Samples were incubated on ice for 20 minutes and then centrifuged at 16.800 g for 20 minutes at 4 °C. After centrifugation, supernatants containing cell lysates were used for Western blotting. Total protein concentration in lysates was assessed using the Bradford Reagent (Bio-Rad, Hercules, California, USA). Three technical

Antigen	Species	Source and catalogue number	Dilution
PYGL	Rabbit	Proteintech, Cat#15851-1-AP	1/1,000
Histone H3	Rabbit	Abcam, Cat# ab201456	1/3,000
GAPDH	Mouse	Santa Cruz Biotechnology, Cat#sc-32233	1/3,000
H3K9Ac	Rabbit	Abcam, Cat# ab4441	1/1,000
H4K5Ac	Rabbit	Santa Cruz Biotechnology, Cat#sc-34264	1/1,000
H4K12Ac	Rabbit	Santa Cruz Biotechnology, Cat#sc-34266	1/1,000
β-actin	Mouse	Novus Biologicals, Cat# NB600-501	1/3,000
p-GYS2 (S641)	Rabbit	Cell Signaling Technology, Cat#3891	1/1,000
GYS2	Rabbit	Cell Signaling Technology, Cat#3886	1/1,000
ASL	Rabbit	Abcam, Cat# ab201026	1/1,000
Vinculin	Mouse	Santa Cruz Biotechnology, Cat#sc-73614	1/3,000

Table 2: List of commercial antibodies used for Western blotting in this study. For each, species, catalogue number and dilution used are indicated.

replicates were used for each sample. Approximately 10 micrograms of whole cell lysates or 5 micrograms of nuclear and cytosolic fractions were run onto SDS-PAGE gels (Bio-Rad, Hercules, California, USA) and transferred onto 0.45 µm polyvinylidene difluoride (PVDF) membranes (Cytiva, Marlborough, USA) at 100 V for 2 hours. Membranes were then blocked using a 5% non-fat milk solution in TBS-Tween-20 for 1 hour at room temperature. Incubation with primary antibodies was done overnight at 4 °C. The primary antibodies used are summarized in **Table 2**. Proteins of interest were detected using horseradish peroxidase (HRP)-conjugated goat anti-mouse or donkey anti- rabbit IgG antibody (GE Healthcare, dilution 1/3000). Peroxidase substrate was provided by LiteAblot PLUS (EuroClone, Pero, Italy). Western blot bands were quantified using ImageJ software (Fiji2).

Immunofluorescence on isolated nuclei

For isolation of intact nuclei, subcellular fractionation was performed as described above. Pellets containing nuclei were resuspended in 4% PFA, instead of nuclear lysis buffer, and they were not sonicated. Immunofluorescence staining was performed on intact nuclei placed on glass coverslips. Prior to permeabilization, negative control slides were treated with 0.5% alpha-amylase in PBS for 20 minutes to digest glycogen. Samples were then permeabilized for 20 min in PBS containing

0.2% Triton® X-100. Blocking solution containing 5% donkey serum was applied for 1 h. Primary antibodies were diluted in blocking solution and incubated overnight at 4°C. Anti-Lamin A (Abcam, Cat#26300) was used at 1:1,000 dilution and anti-glycogen (kind gift from O. Baba) (Baba, 1993) was used at 1:50 dilution. Next, slides were washed three times in PBS for 5 min each and then incubated with fluorescently labeled secondary antibodies. The secondary antibody Anti-chicken Fluor® 488, and anti-rabbit Alexa Fluor® 594 were used at 1:400 dilutions. Sections were washed three times in PBS for 5 min each and mounted on glass slides with Vectashield (Vector Laboratories, Burlingame, CA) mounting reagent. Images were obtained using ZEISS LSM 700 confocal microscope (Zeiss, Oberkochen, Germany).

Nuclear metabolite measurements

Metabolites were assessed in nuclear enriched fractions obtained as described above. Acetyl CoA concentrations were determined by using a fluorometric assay kit (Abcam; Cat#ab87546) according to the manufacturer's instructions. Glucose-6P and dihydroxyacetone-P/glyceraldehyde-3P (DHAP/GAP) concentrations were obtained by liquid chromatography coupled to tandem mass spectrometry using an API-3500 triple quadrupole mass spectrometer (AB Sciex, Framingham, MA, USA) coupled with an ExionLC™ AC System (AB Sciex, Framingham, MA, USA) as previously reported (Audano *et al.*, 2021).

Pathology

Fresh liver samples from *Asl*$^{Neo/Neo}$ mice were fixed in 4% paraformaldehyde for 12 hours, washed twice with 1X PBS and stored at 4 °C in 70% ethanol. Fixed samples were dehydrated by passaging in 95% ethanol over-day and 100% ethanol overnight at 4 °C. Dehydrated samples were then embedded into liquid paraffin. For hematoxylin-eosin (H&E) staining, 5 µm sections were treated following standard protocols. Briefly, sections were dewaxed and rehydrated through graded alcohol solutions to water. Samples were then stained with Harris hematoxylin for 30 seconds, washed for 10 minutes in running tap water and then counterstained with aqueous eosin (1% solution) for 30 seconds. Stained sections were dehydrated with ethanol, cleared in xylene and mounted. Glycogenated nuclei were quantified from H&E sections. A minimum amount of 1,000 nuclei were used for quantification.

Enzyme activity assays

GYS2 activity was determined using a commercially available colorimetric assay (Cohesion Biosciences, London, UK, Cat#CAK1168) on nuclear purified fractions according to the manufacturer's instructions and normalized for protein concentrations in nuclear extracts. Results were expressed as units per milligram (U/mg). Histone acetyltransferase (HAT) activity was determined using a commercially available assay (Sigma-Aldrich, St. Louis, MO, USA, Cat#EPI001-1KT) on nuclear purified fractions according to the manufacturer's instructions and normalized for protein concentrations. Histone deacetylase (HDAC) activity was determined using a commercially available fluorometric assay (Sigma-Aldrich, St. Louis, MO, USA, Cat#CS1010-1KT) on nuclear purified fractions according to the manufacturer's instructions and normalized for protein concentrations.

Glycogen determination

Liver glycogen storage was assessed using commercially available glycogen assay kit (Sigma-Aldrich, St. Louis, MO, USA, Cat#MAK016-1KT). Briefly, 10 mg of liver tissue were homogenized on ice in 200 µl of water and boiled for 10 minutes to inactivate enzymes. Samples were subsequently centrifuged at 18,000 x g for 10 minutes. The glycogen containing supernatant was used for the assay. Glycogen was quantified measuring the absorbance at 570 nm. A curve made with known concentrations of glycogen was used as a standard. Hepatic glycogen levels were normalized for protein concentrations determined by Bradford reagent (Bio-Rad, Hercules, California, USA).

Biotin-switch assay for S-nitrosylated protein detection

The biotin-switch assay was performed using a commercially available S-nitrosylated protein detection assay kit (Abcam, Cat#236207) according to the manufacturer's instructions. Briefly, 30 mg of liver tissue were lysed in S-nitrosylation wash buffer supplemented with protease and phosphatase inhibitor cocktails (Complete and PhosSTOP Roche, Roche Diagnostics, Basel, Switzerland) and homogenized as described for whole cell lysates. After lysis, free thiol (-SH) groups in lysates were first blocked, then any nitrosylated sulphurs (S-NO) were cleaved, reduced to -SH and finally biotinylated. Samples treated with no reducing buffer and thus non biotinylated were used as negative controls. For PYGL immunoprecipitation, 500 micrograms of whole liver

lysates were incubated with 5 micrograms of anti-PYGL antibody (**Table 2**) over-night. Lysates were then incubated with 30 µl of DynaBeads Protein G (ThermoFisher, Waltham, MA, USA; Cat# 10004D) for two hours at 4°C, washed three times with 0.02% Tween-20 in PBS and loaded onto SDS-PAGE gels as described above. S-nitrosylated cysteine was detected using an anti-biotin HRP conjugated antibody (Cell Signaling Technology, Cat#7075).

RNA extraction, reverse transcription and qPCR

Total RNA from livers was extracted using RNeasy mini kit (Qiagen). One microgram of RNA was retro-transcribed using High-Capacity cDNA Reverse Transcription Kit (Applied Biosystems). The qPCR reactions were set up using SYBR Green Master Mix and run in triplicate on a Light Cycler 480 System (Roche). The primer sequences for mouse *Pygl* were: forward, 5′-ggcagaagtggtgaacaatgacc-3′; and reverse, 5′-tccgataggtctgtggctggaa -3′. The primer sequences for mouse *Cd36* were: forward, 5'-atgggctgtgatcggaactg-3'; and reverse, 5'-tttgccacgtcatctgggttt-3'. The primer sequences for mouse *Pparg* were: forward, 5'-gtactgtcggtttcagaagtgcc-3'; and reverse, 5'-atctccgccaacagcttctcct-3'. The primer sequences for mouse Beta actin were: forward, 5'-ggctgtattcccctccatcg-3'; and reverse, 5'-ccagttggtaacaatgccatgt-3'. The primer sequences for mouse Beta 2 microglobulin were: forward, 5'-tggtgcttgtctcactgacc-3'; and reverse, 5ì-gtatgttcggcttcccattc-3'. Running program was as follows: pre-heating, 5 min at 95 °C; 40 cycles of 15 s at 95 °C, 15 s at 60 °C, and 25 s at 72 °C. Beta actin was used as housekeeping gene in the qPCR for *Pygl*. Beta 2 microglobulin was used as housekeeping gene in the qPCRs for *Pparg* and *Cd36*. Data were analyzed by LightCycler 480 software version 1.5 (Roche).

Quant-Seq analysis

Gene expression analysis was performed on WT and $Asl^{Neo/Neo}$-mice (n = 5 per group). Total RNA from frozen livers was extracted according to the manufacturer's instructions (RNeasy Mini Kit, Cat No./ID: 74106 (250), Qiagen). Total RNA was quantified using the Qubit 4.0 fluorimetric Assay (Thermo Fisher Scientific). Libraries were prepared from 125 ng of total RNA using the NEGEDIA Digital mRNA-seq research grade sequencing service (Next Generation Diagnostic srl) (Xiong *et al.*, 2017) which included library preparation, quality assessment and sequencing on a NovaSeq 6000 sequencing system using a single-end, 100 cycle strategy (Illumina Inc.). Illumina NovaSeq 6000 base call files were converted into fastq file through bcl2fastq; Trimming and

cleaning with bbduk; Alignment was performed with STAR 2.6.0a. The expression levels of genes were determined with HTseq-counts 0.9.1. The reference genomes were Hg38 and rn6. The raw data were analyzed by Next Generation Diagnostic srl proprietary NEGEDIA Digital mRNA-seq pipeline (v2.0) which involves a cleaning step by quality filtering and trimming, alignment to the reference genome and counting by gene (Anders *et al.*, 2015). The raw expression data were normalized, analyzed, and visualized by Rosalind HyperScale architecture OnRamp BioInformatics, Inc. In this statistical analysis the threshold for statistical significance chosen was a false discovery rate of ≤0.05. For differential expression analysis, an additional threshold was used: logFC ≥2 for upregulated genes and logFC ≤−2 for downregulated genes.

Functional analysis of transcriptomic data

The list of 1145 deregulated genes considering the logFC≥2 was crossed with the list of peaks obtained by the Experiment ENCSR000CEQ publicly available in the Encyclopedia of DNA Elements (ENCODE) project (ENCODE project consortium, 2012. The list of peaks was cut to restrict the promoter region to a 3kb region which includes the peaks located 2.5 kb upstream and 0.5 kb downstream the transcription start site (TSS). The overlap with the list of deregulated genes was high: 86% (989/1145) of the induced genes presents at least one acetylated lysine 9 of histone 3 (H3K9Ac) positive peak in the mouse liver. Data from RNA sequencing were analyzed by using the DAVID online tool (DAVID Bioinformatics Resources 6.8), for the "Kyoto Encyclopedia of Genes and Genomes" (KEGG Pathway) analyses. The analysis was performed on induced and inhibited genes, separately. The threshold for statistical significance for the KEGG Pathway analysis was FDR≤10%. Venn diagram was generated using custom annotation script.

Statistical analyses

Data were analyzed using GraphPad Prism 5.0 software (San Diego, CA, USA). Comparisons of continuous variables between two and more experimental groups were performed using the two-tailed unpaired Student's t-test or one-way ANOVA with Tukey's post hoc tests, respectively. Kaplan–Meier survival curves were compared using the log-rank test. No statistical methods were used to predetermine the sample size. No formal randomization procedure was used but assignment of mice to treatment groups was based on mouse identification numbers, and the investigators were not blinded. The number of replicates is reported in the Figure legends. Data

are expressed as means ± SEM. P-values < 0.05 were considered statistically significant.

RESULTS

Nuclear glycogen accumulation in the liver is a feature of argininosuccinic aciduria.

Glycogen storage in the liver has been previously reported in ASA (Bigot *et al.*, 2017; Burrage *et*

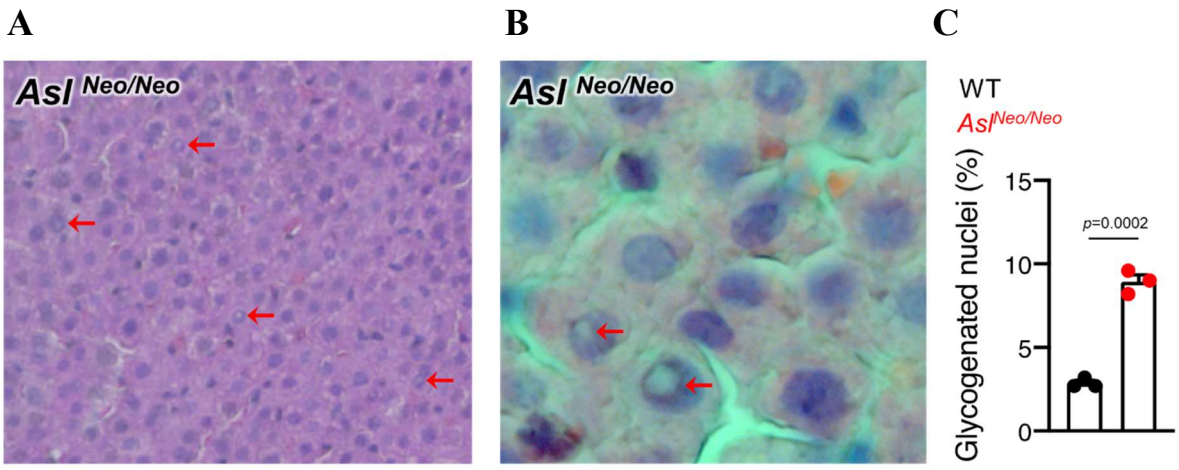

Fig. 8: (A) Hematoxylin and eosin staining of livers of *Asl*$^{Neo/Neo}$ mice. Red arrows point to glycogenated nuclei, visible as white nuclear pseudo-inclusions. **(B)** Higher magnification showing glycogenated nuclei (red arrows). **(C)** Quantification of glycogenated nuclei in *Asl*$^{Neo/Neo}$ (red) or WT (black) mice. Quantification was performed on >1000 nuclei (n=3/mice per group). Student's t-test was used for P-value calculation.

al., 2020; Yaplito-Lee *et al.*, 2013). Previous work from our group showed that glycogen deposition does not only occur in the cytoplasm, but also in the nucleus (Soria *et al.*, 2021). This finding was confirmed by electron microscopy of the liver of *Asl*$^{Neo/Neo}$ mice, a murine model of ASA (Erez *et al.*, 2011). By hematoxylin-eosin staining of livers of *Asl*$^{Neo/Neo}$ mice about 10% of

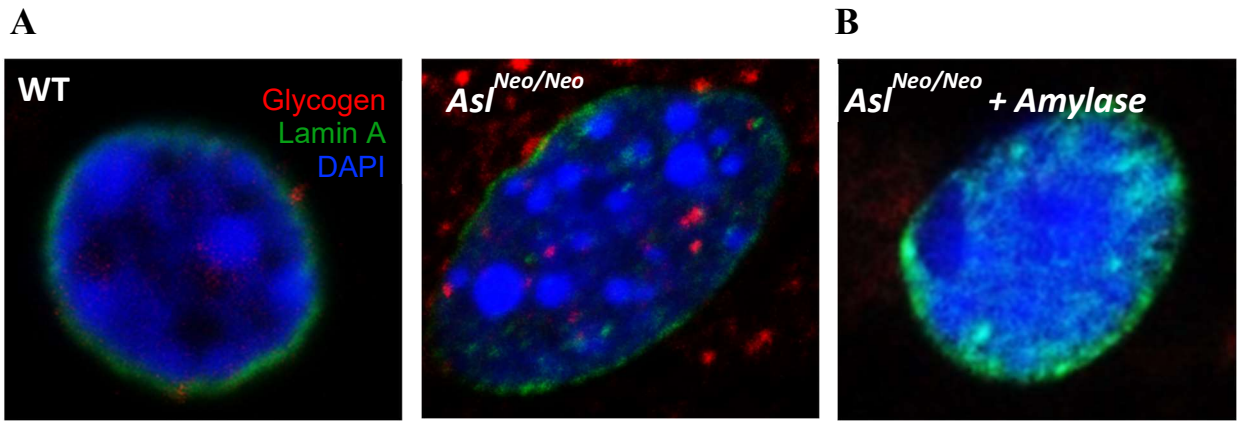

Fig. 9: (A) Immunofluorescence on isolated nuclei from wild type (WT), or *Asl*$^{Neo/Neo}$ mouse livers. Nuclear content is stained by DAPI (blue); nuclear membrane is shown in green (Lamin A); glycogen is shown in red. **(B)** Loss of glycogen staining in nuclei isolated from the livers of *Asl*$^{Neo/Neo}$ mice after treatment with the glycogen-catabolizing enzyme alpha-amylase.

glycogenated nuclei were observed, a percentage significantly higher than WT controls (**Figure**

8). Immunofluorescence with an antibody that specifically recognizes glycogen (Baba, 1993) on isolated nuclei confirmed increased glycogen in livers of *Asl*$^{Neo/Neo}$ mice compared to WT controls (**Figure 9A**). The fluorescence signal disappeared upon treatment with alpha-amylase, an enzyme that can digest glycogen, confirming that the fluorescent signal was indeed glycogen (**Figure 9B**). Electron microscopy analysis on liver biopsies from two patients with ASA confirmed the nuclear glycogen storage is also present in humans (**Figure 10**).

Impaired glycogenolysis drives metabolic and epigenetic changes.

Glycogen is synthesized *de novo* and degraded in the nucleus, without direct exchange of glycogen between this compartment and the cytoplasm (Sun *et al.*, 2019). Western blotting on nuclear fractions isolated from the livers of *Asl*$^{Neo/Neo}$ mice and WT controls showed a significant reduction in the relative abundance of PYGL, the first and rate-limiting enzyme of the glycogenolytic pathway (**Figure 11A-B**). Consistent with previous studies (Burrage *et al.*, 2020), we found reduced abundance of PYGL protein and mRNA (**Figure 11C**). Conversely, relative abundance

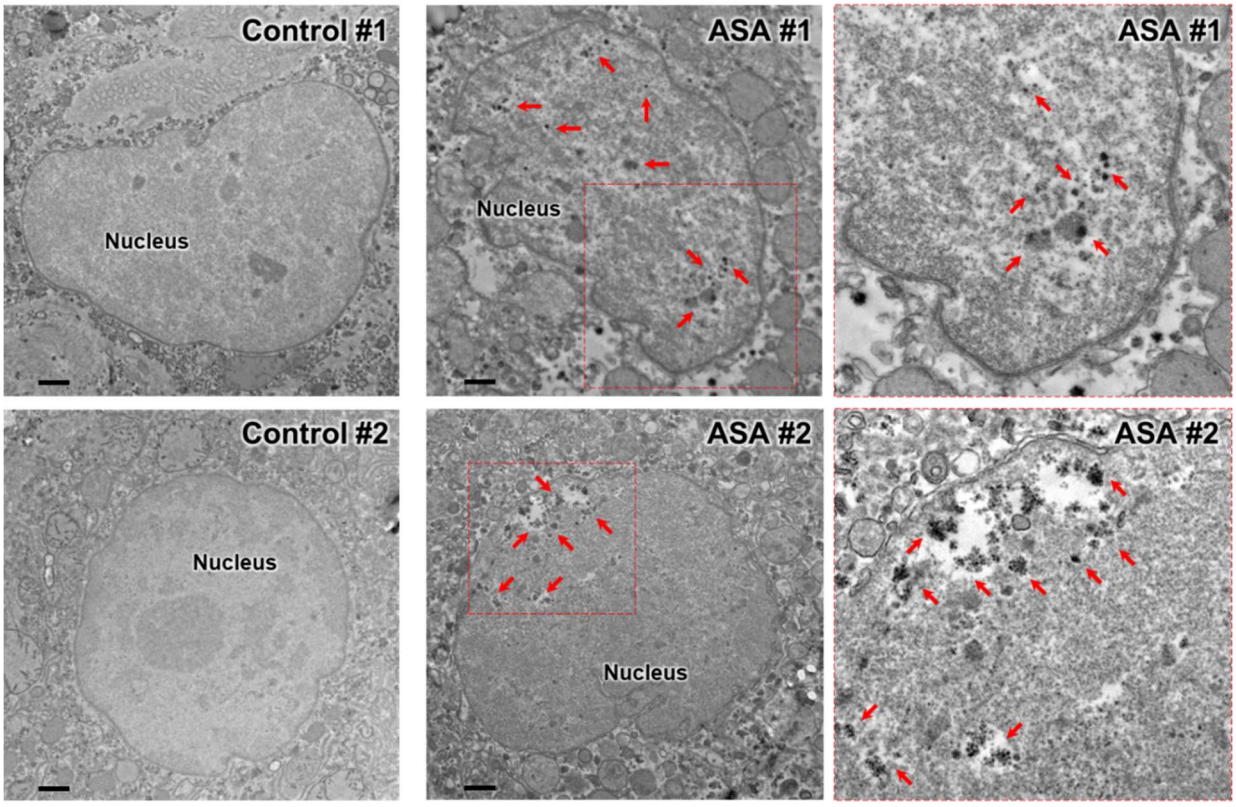

Fig. 10: Electron microscopy showed nuclear glycogen in the livers of two patients (ASA #1 and ASA #2) with ASA but not in the controls; the zones in the red boxes are shown at higher magnifications in the right panels. Red arrows indicate glycogen.

of GYS2, the rate-limiting enzyme for glycogen synthesis, were unaffected in both whole cell lysates and nuclear extracts (**Figure 11D-G**).

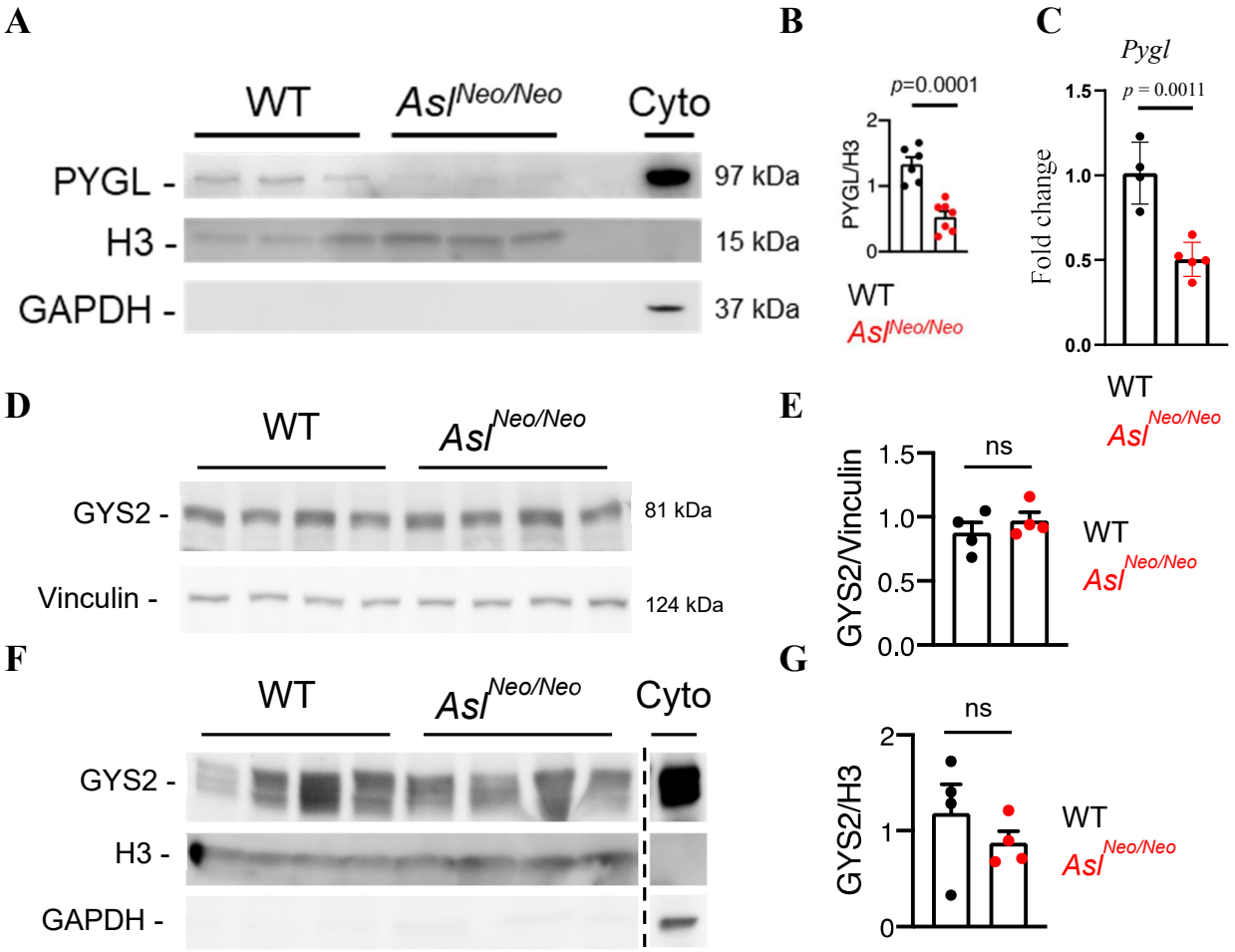

Fig. 11: (A) Western blotting on nuclear extracts from livers of WT or *Asl*$^{Neo/Neo}$ mice for PYGL. Histone H3 was used as a loading control. GAPDH was used as control of the purity of the nuclear extracts. One cytosolic fraction sample (Cyto) is shown as control. **(B)** Quantification of relative abundance of PYGL in nuclear fractions. **(C)** qPCR analysis of *Pygl* in livers of *Asl*$^{Neo/Neo}$ mice compared to WT controls (n = 4-5 mice/group). **(D)** Western blotting on whole cell lysates from livers of WT or *Asl*$^{Neo/Neo}$ mice for GYS2. Vinculin was used as loading control. **(E)** Quantification of GYS2 bands in whole cell lysates. **(F)** Western blotting on nuclear extracts from livers of WT or *Asl*$^{Neo/Neo}$ mice for GYS2. Histone H3 was used as a loading control. GAPDH was used as a control for nuclear extracts purity. One cytosolic fraction sample (Cyto) is shown as control. **(G)** Quantification of GYS2 bands in nuclear fractions. Student's t-test was used for P-value calculation.

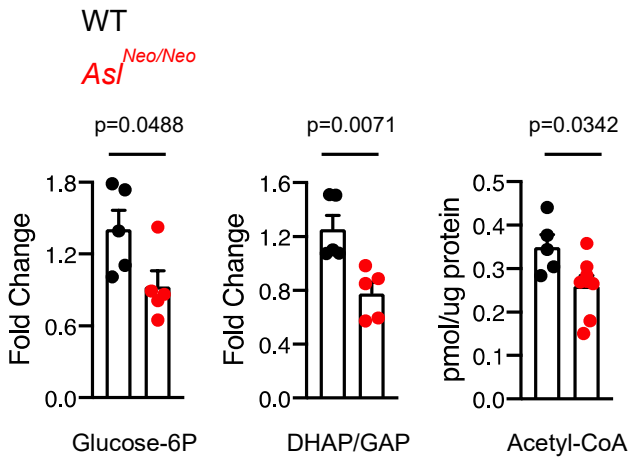

Fig. 12: Quantification of metabolites in liver nuclear extracts of WT (black) and *Asl*$^{Neo/Neo}$ (red) mice (n=5-6/mice per group). Student's t-test was used for p-value calculation.

Glycogenolysis started by PYGL generates glucose which is converted into acetyl-CoA. The nuclear and cytoplasmic pools of acetyl-CoA are separated because acetyl-CoA cannot cross the nuclear membrane and has to be synthesized in the nucleus (Bulusu *et al.*, 2017). In the nuclei of ASA mice, we found reduced glycolysis intermediates, such as glucose-6-phosphate (Glucose-6P) and dihydroxyacetone-phosphate/glyceraldehyde-3-phosphate (DHAP/GAP), and acetyl-CoA (**Figure 12**).

Acetyl-CoA is a donor of acetyl groups for histone acetyltransferases (HAT) (Shvedunova and Akhtar, 2022) and reduced nuclear acetyl-CoA results in decreased histone acetylation (Sun *et al.*, 2019). Western blotting with antibodies recognizing various histone acetylation marks showed a significant reduction of histone acetylation in *Asl*$^{Neo/Neo}$ mice (**Figure 13**). The activities of the HATs was unaffected and the activity of histone deacetylases (HDACs), that remove acetyl group from histones, was not increased in *Asl*$^{Neo/Neo}$ mice (**Figure 14**), thus excluding changes in the activities of these two enzymes.

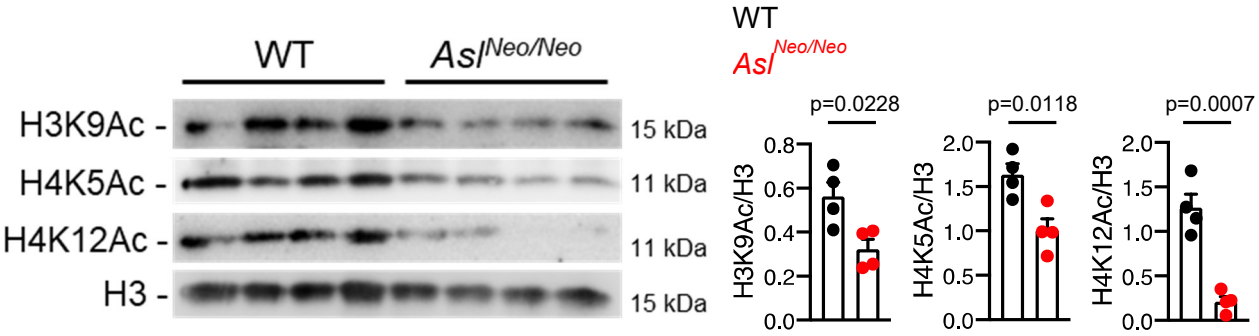

Fig. 13: Western blotting on nuclear extracts of livers of WT or *Asl*$^{Neo/Neo}$ mice for H3K9Ac, histone H4, lysine 5 (H4K5Ac) and histone H4, lysine 12 (H4K12Ac). Histone H3 was used as a loading control. Quantification of acetylated histone acetylation bands is shown on the right (n=4/mice per group). Student's t-test was used for p-value calculation.

In contrast to livers, Western blotting on nuclear fractions of brain and muscle showed no changes

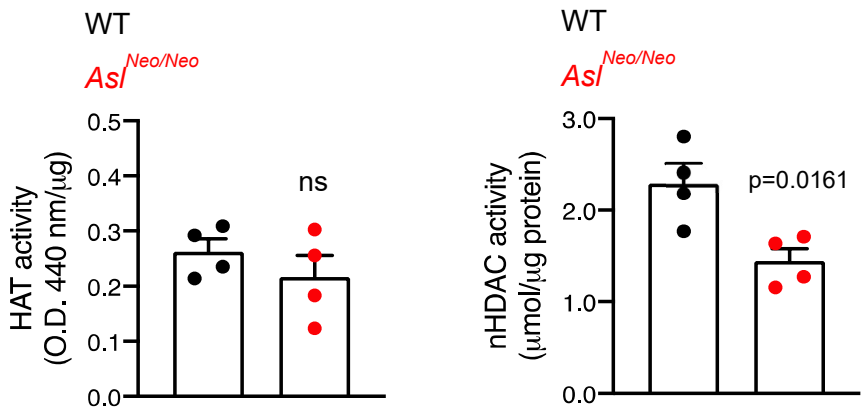

in histone acetylation alterations in *Asl*$^{Neo/Neo}$ mice (**Figure 15**).

Fig. 14: Activity of histone acetyltransferases (HAT) and histone deacetylases (HDAC) in nuclear extracts of WT and *Asl*$^{Neo/Neo}$ mouse livers (n=4/mice per group). Student's t-test was used for p-value calculation. ns: not statistically significant.

Nuclear glycogen is not detected in other UCDs or other GSDs.

To investigate whether nuclear glycogen was also present in other UCDs, we evaluated livers of ornithine transcarbamylase deficient mice (*Spf-ash* mouse, Soria *et al.*, 2021), and argininosuccinate synthetase 1 deficient mice (*Ass1*^{Fold}, ASS1 LiKO; Lisjak *et al.*, 2023; Keshet *et al.*, 2020) by electron microscopy that did not detected any nuclear glycogen (**Figure 16**) and by western blotting that revealed no changes in histone acetylation compared to controls (**Figure 17**).

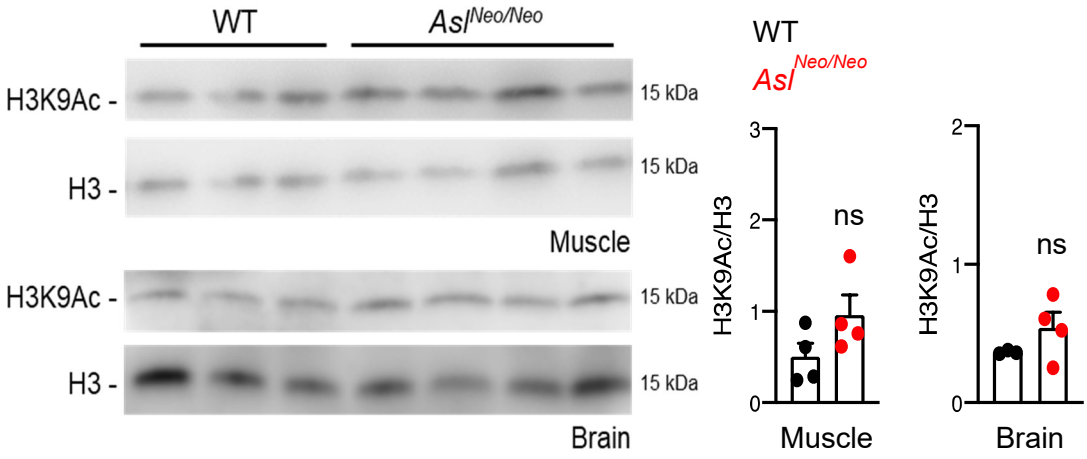

Fig. 15: Western blotting on nuclear extracts from muscle or brain of WT or *Asl*$^{Neo/Neo}$ mice for H3K9Ac. Histone H3 was used as a loading control. Quantification of Western blot bands is shown on the right panel. Student's t-test was used for p-value calculation (n=4/mice per group). ns: not statistically significant.

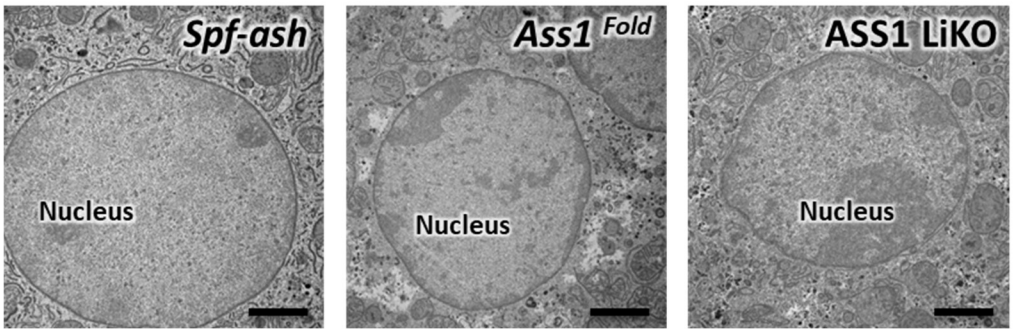

Fig. 16: Electron microscopy of livers from three mouse models of UCDs show no glycogen in the nuclei. *Spf-ash*, ornithine transcarbamylase-deficient mice; *Ass1*^{Fold}, argininosuccinate synthetase 1 deficiency; *ASS1 LiKO*, liver-specific knockout of argininosuccinate synthetase 1.

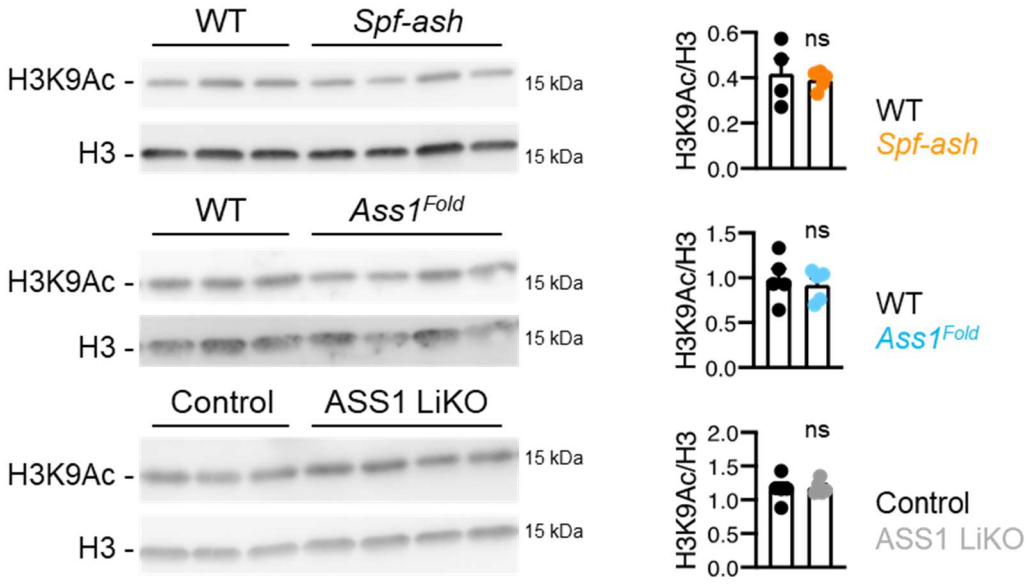

Fig. 17: Western blotting on nuclear extracts of livers of WT or various mouse models of UCDs for H3K9Ac. Histone H3 was used as loading control. Quantification of western blot bands is shown on the right. Student's t-test was used for p-value calculation (n=4-5/mice per group). ns: not statistically significant. Spf-ash, ornithine transcarbamylase-deficient mice; Ass1Fold, hypomorphic model of argininosuccinate synthetase 1 deficiency; ASS1 LiKO, liver-specific knockout of argininosuccinate synthetase 1.

Next, we evaluated livers of several GSD mouse models (Gümüş and Özen, 2023), including a liver-specific glucose-6-phosphatase alpha deficiency (*L-G6pc*$^{-/-}$, Mutel *et al.*, 2011), acid maltase deficiency (*Gaa*$^{-/-}$, Tarallo *et al.*, 2021) and glycogen debranching enzyme deficiency (*Agl*$^{-/-}$, Vidal *et al.*, 2018). Although livers of these mice all showed abundant glycogen storage in the cytoplasm or lysosome, nuclear deposition of glycogen was not detected by electron microscopy, in contrast

to *Asl*$^{Neo/Neo}$ mouse livers (**Figure 18**). Consistently, histone acetylation was unaffected (**Figure 19**).

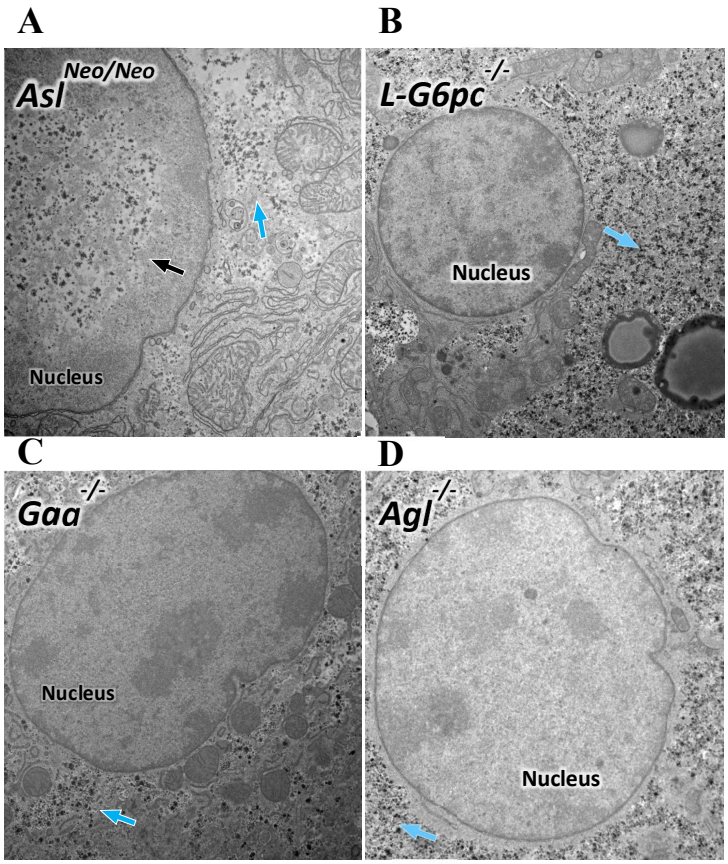

Fig. 18: (A) Electron microscopy of the liver of an *Asl*$^{Neo/Neo}$ mouse. The light blue arrow indicates glycogen deposits, visible as black dots, in the cytoplasm; black arrows indicate glycogen storage in the nucleus. **(B)** Electron microscopy of the liver of a mouse model of liver-specific *G6pc* deficiency (GSD Ia). **(C)** Electron microscopy of the liver of a murine model of Pompe disease (GSD II). **(D)** Electron microscopy of the liver of a murine model of *Agl* deficiency (GSD III).

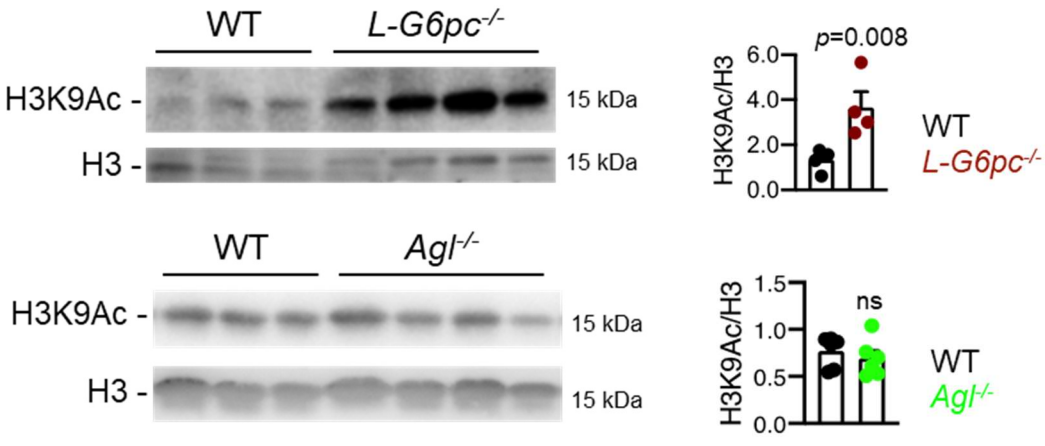

Fig. 19: Western blotting on nuclear extracts of livers of WT or various GSD mouse models for H3K9Ac. Histone H3 was used as loading control. Quantification of Western blot bands is shown on the right. Student's t-test was used for p-value calculation (n=3-6/mice per group). ns: not statistically significant.

Despite the massive cytosolic deposition, nuclear glycogen was also not detected in a mouse model of Hers disease (GSD VI) with complete deficiency of PYGL (Wilson *et al.*, 2019) (**Figure 20A**). Consistently, Western blotting on nuclear extracts showed unaffected histone acetylation (**Figure 20B-C**).

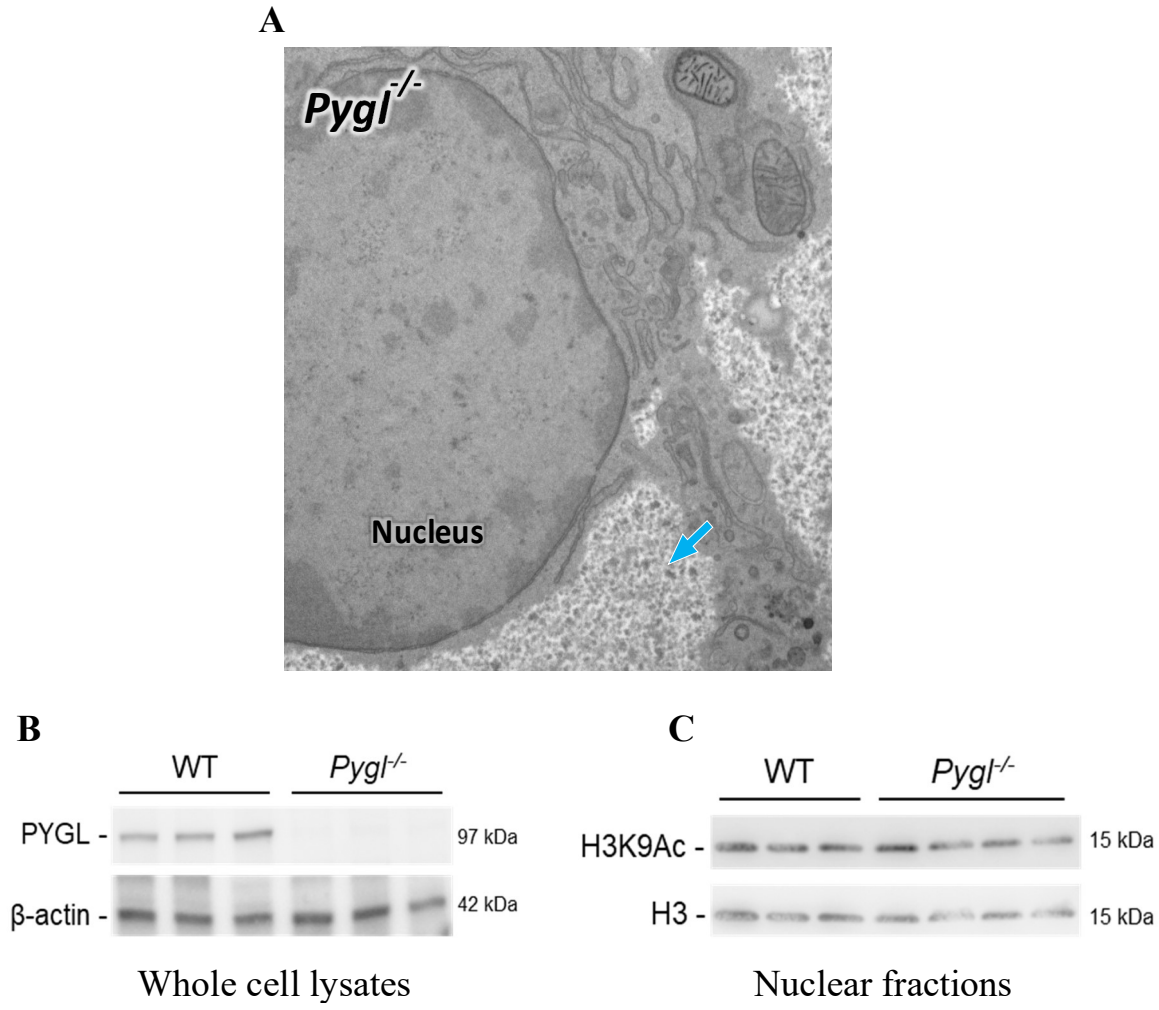

Fig. 20: (A) Electron microscopy of the liver of a mouse model of PYGL deficiency (GSD VI). The light blue

arrow points to glycogen accumulation, visible as black dots, in the cytoplasm. **(B)** Western blotting for PYGL of whole cell lysates from the livers of WT or PYGL-deficient mice. β-actin was used as loading control. **(C)** Western blotting of nuclear extracts for H3K9Ac on livers of WT or PYGL-deficient mice . Histone H3 was used as loading control.

To explain this relevant difference between *Asl*$^{Neo/Neo}$ and *Pygl*$^{-/-}$ mice, we investigated nuclear glycogenesis by monitoring the levels of GYS2. However, although the protein amount was unaffected, GYS2 was hyperphosphorylated on Serine 641 and the enzyme activity was reduced in *Pygl*$^{-/-}$ mice (**Figure 21A-B**). The increased phosphorylation of GYS2 that inhibits the catalytic activity of the enzyme, that is the rate limiting step on glycogen synthesis (Wilson *et al.*, 2005) might be responsible for the lack of nuclear glycogen storage in *Pygl*$^{-/-}$ mice.

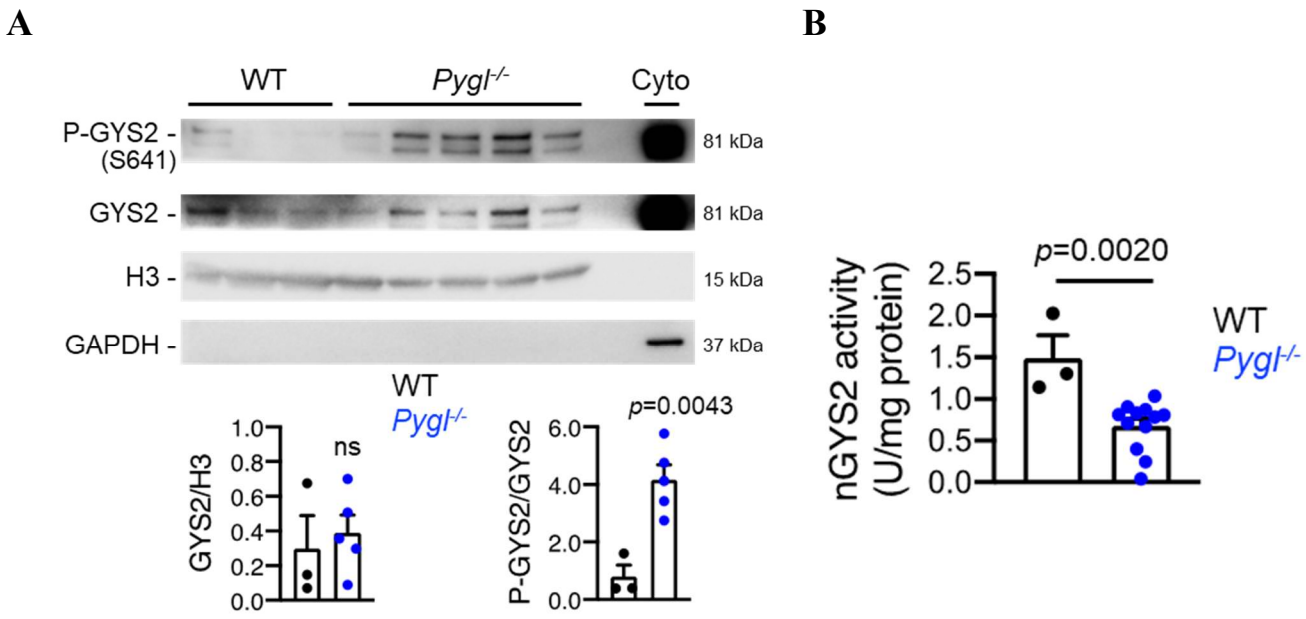

Fig. 21: (A) Western blotting on nuclear fractions on livers of WT (n=3) or *Pygl*$^{-/-}$ (n=5) for GYS2 phosphorylated on Serine 641 (S641), and total GYS2. Cytosolic fraction (Cyto) from one of the samples is shown as control. Histone H3 was used as a loading control and GAPDH to evaluate the purity of nuclear fractions. Quantifications of Western blot bands are shown. **(B)** Enzymatic activity of GYS2 in nuclear fractions of livers of WT (n=3) or *Pygl*$^{-/-}$ (n=12) mice. Student's t-test was used for p-value calculation. ns: not statistically significant.

Epigenetic changes and changes in liver homeostasis in *Asl*$^{Neo/Neo}$ mice.

Histone acetylation is a key regulator of gene expression (Verdone *et al.*, 2005) and to investigate the changes induced by histone hypoacetylation in livers of *Asl*$^{Neo/Neo}$ mice, we performed RNA-sequencing that detected 1,145 differentially expressed genes (DEGs), with 45% of them upregulated and 55% down-regulated (**Figure 22**).

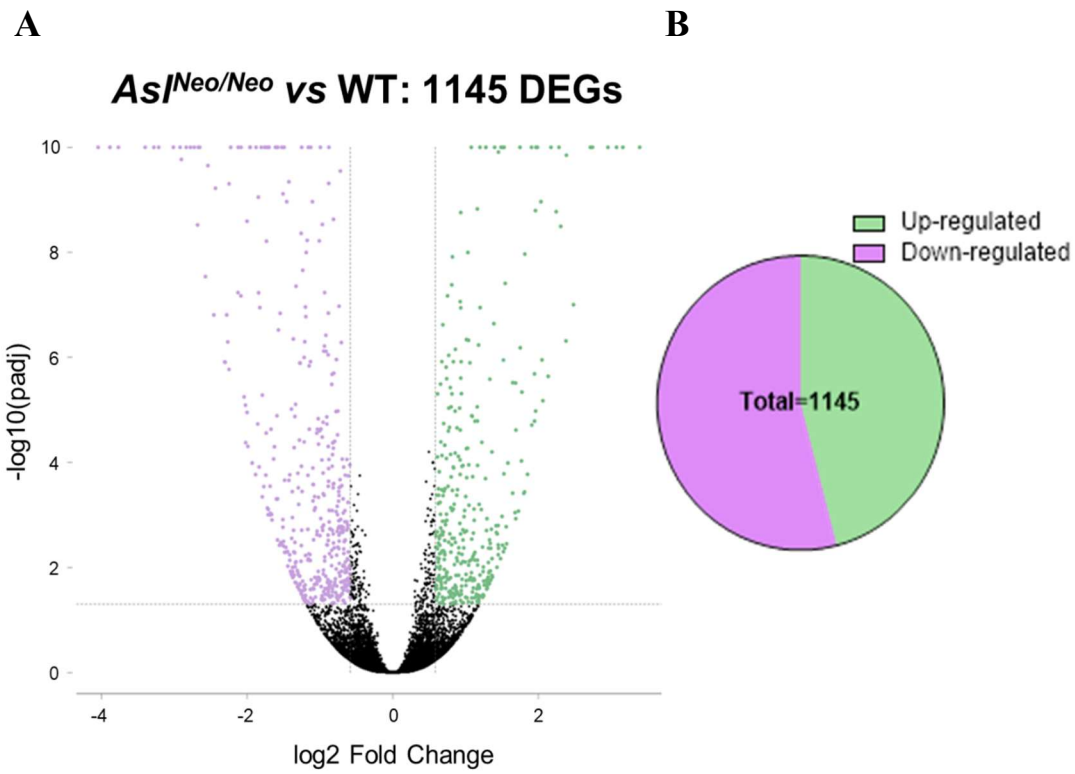

Fig. 22: Volcano plot showing differentially expressed genes (DEGs) between WT and *Asl*$^{Neo/Neo}$ mouse livers. **(B)** Pie chart with percentages of upregulated and downregulated genes in *Asl*$^{Neo/Neo}$ mouse livers.

The striking majority of DEGs in *Asl*$^{Neo/Neo}$ mice overlapped with an independent dataset of genes of the ENCODE project consortium (ENCODE Project Consortium, 2012) that included genes regulated in livers of WT mice-by acetylation of lysine 9 of histone H3 (**Figure 23**). This data supports the hypothesis that liver transcriptomic changes in *Asl*$^{Neo/Neo}$ mice are largely driven by histone hypoacetylation.

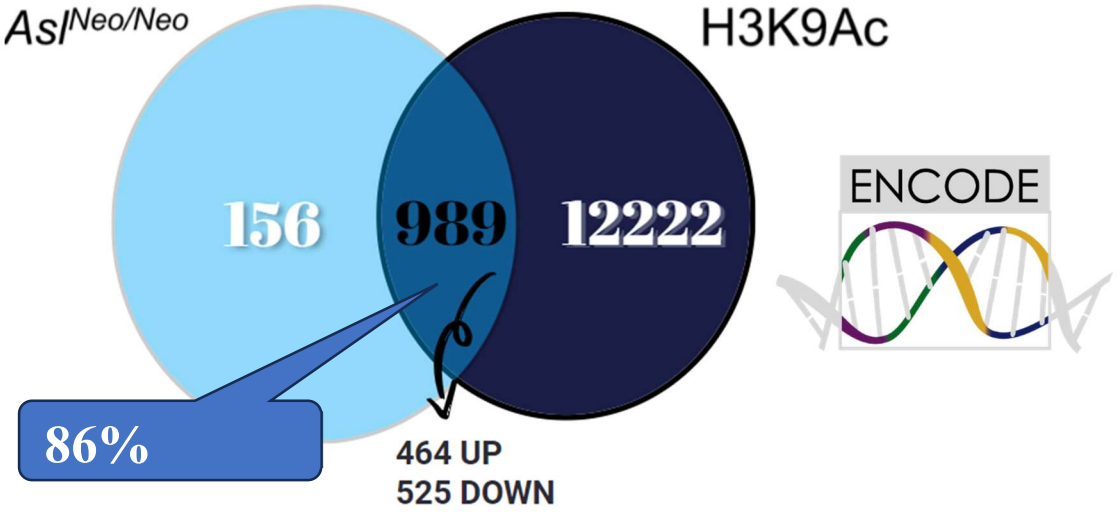

Fig. 23: DEGs in livers of *Asl*$^{Neo/Neo}$ mice regulated by H3K9Ac.

Hepatic delivery of PYGL and treatment with HDACi in *Asl*$^{Neo/Neo}$ mice

To correct histone hypoacetylation in *Asl*$^{Neo/Neo}$ mice, we investigated two independent approaches: AAV-mediated delivery of PYGL (AAV-PYGL) or treatment with SAHA, a HDACi (**Figure 24**).

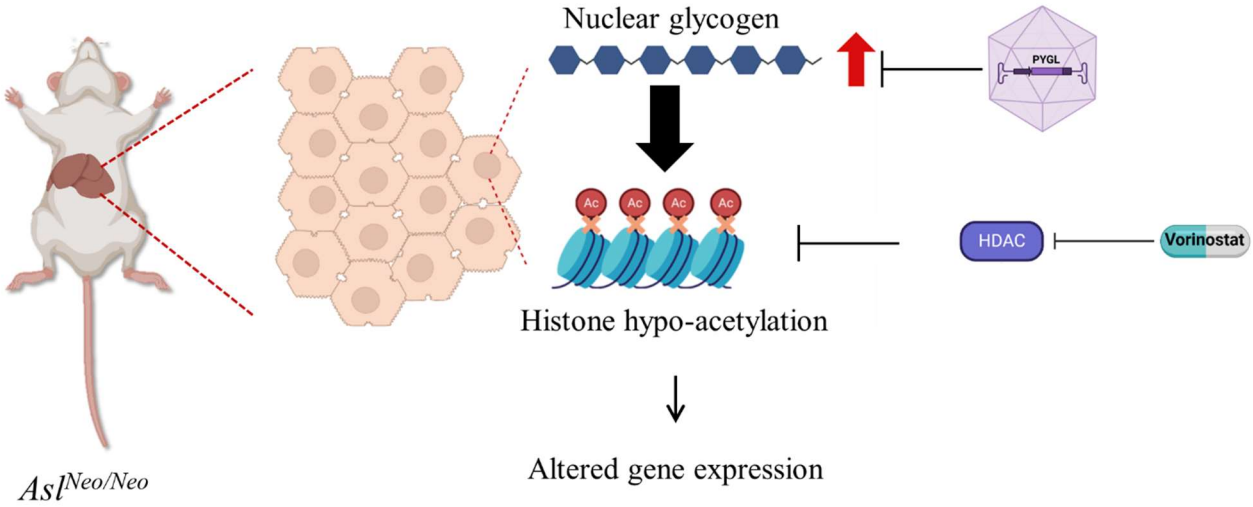

Fig. 24: Schematic depiction of the working model for the two therapeutic strategies investigated in this work to counteract the effect of histone hypoacetylation induced by increased nuclear glycogen storage: AAV-mediated delivery of PYGL to hepatocytes and HDACi treatment by SAHA.

Before testing in the *Asl*$^{Neo/Neo}$ mice, the AAV-PYGL was first injected at a dose of $1x10^{13}$ GC/kg in WT mice and Western blotting on liver lysates confirmed overexpression of PYGL in both cytosolic and nuclear fractions of livers (**Figure 25A**) and a reduction in liver glycogen content

was also observed (**Figure 25B**).

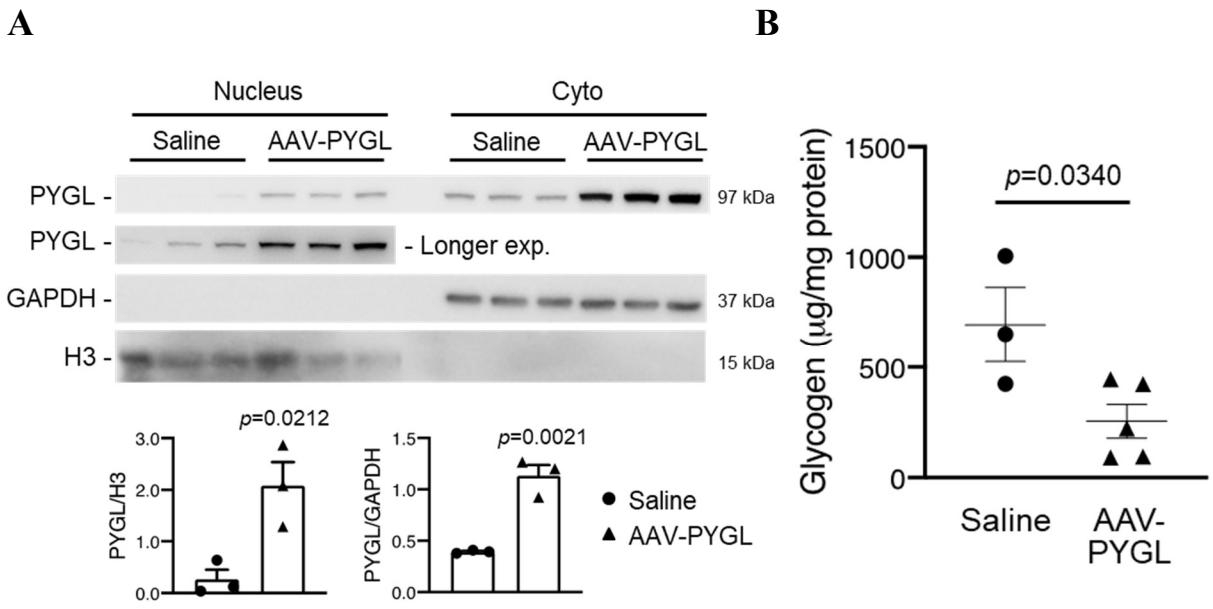

Fig. 25: (A) Western blotting for PYGL on nuclear and cytosolic extracts of livers of WT mice injected with either an AAV vector expressing the human PYGL (AAV-PYGL) or saline. Histone H3 and GAPDH were used as loading and fraction purity controls. **(B)** Liver glycogen content in livers of WT mice injected with either AAV-PYGL or saline solution. Student's t-test was used for p-value calculation (n=3-5 mice/group).

Next, *Asl*$^{Neo/Neo}$ mice were either injected intravenously with AAV-PYGL or received SAHA by i.p. injections, in addition to a standard therapy (ST), consisting of daily i.p. injections of arginine and sodium benzoate starting from 10 days of life. Control *Asl*$^{Neo/Neo}$ mice receiving only ST. Notably, both treatments significantly improved survival of *Asl*$^{Neo/Neo}$ mice and increased histone acetylation in liver compared to mice receiving ST alone without changes in ASL expression (**Figures 26 and 27**).

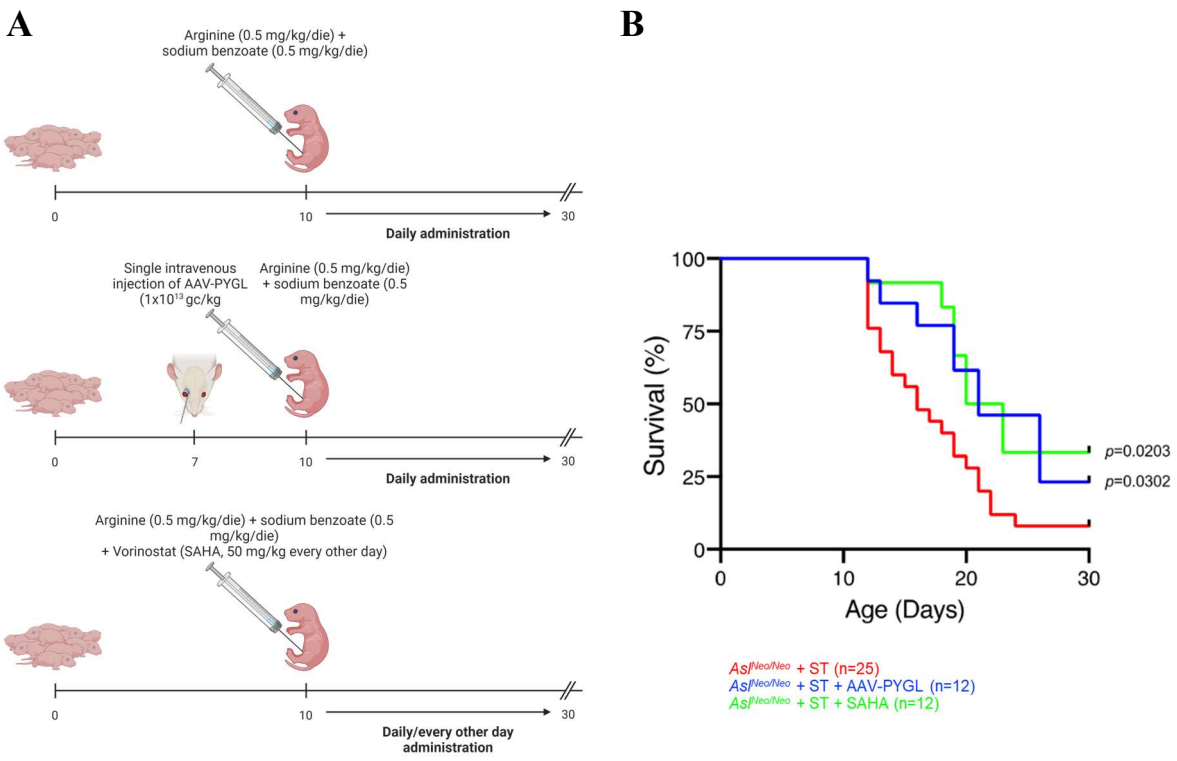

Fig. 26: (A) Scheme of the experimental plan: *Asl*$^{Neo/Neo}$ mice received daily i.p. administration of arginine (0.5 mg/kg/die) and sodium benzoate (0.5 mg/kg/die) starting from 10 days of age (standard therapy, ST), and were then treated with either a single i.v. injection of AAV-PYGL (1x10^{13} gc/kg) at the age of 7 days, or i.p. injections of SAHA every other day starting from 10 days of age (SAHA, 50 mg/kg). Mice treated with ST alone were used as a control group. **(B)** Kaplan-Meier survival curve comparing the three experimental groups. Log-rank (Mantel-Cox) test was used for p-value calculation.

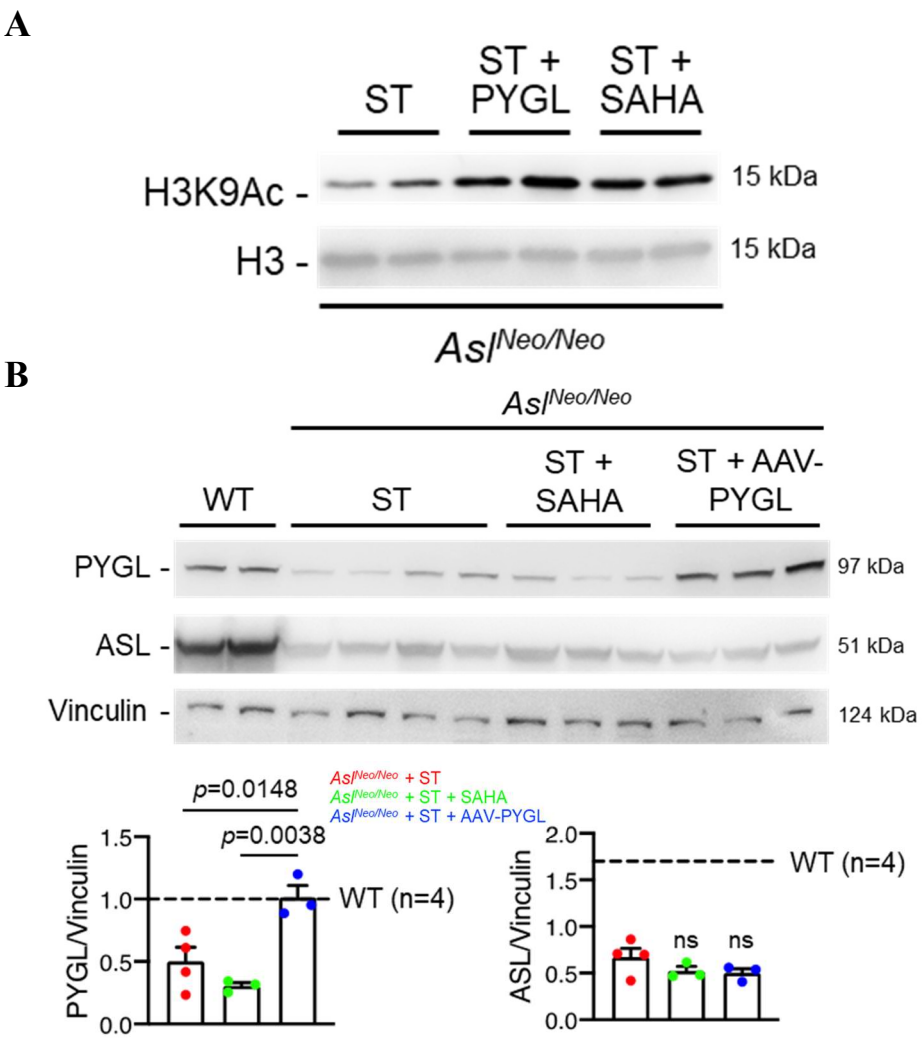

Fig. 27: (A) Western blot for H3K9Ac on nuclear fractions of livers of *Asl*$^{Neo/Neo}$ mice treated with arginine and sodium benzoate (ST), ST and overexpression of PYGL (ST + AAV-PYGL), and ST + vorinostat (ST + SAHA), using an antibody against. Histone H3 was used as loading control. (B) Western blot for PYGL and ASL on whole liver lysates of *Asl*$^{Neo/Neo}$ mice treated with ST, ST + SAHA, and ST + AAV-PYGL. Vinculin was used as loading control. Western blot band quantifications are shown. Student's t-test was used for p-value calculations (n=3-4 mice/group). ns: not statistically significant.

Nuclear glycogen storage affects lipid metabolism.

Among DEGs in *Asl*$^{Neo/Neo}$ mouse livers a significant up-regulation of genes involved in NAFLD, that has been recently renamed as Metabolic dysfunction-associated fatty liver disease (MAFLD) was detected (**Figure 28**). This finding was particularly interesting given that steatohepatitis is among the few conditions in which glycogenated nuclei have been reported (Takahashi and Fukusato, 2014). Among the up-regulated genes of *Asl*$^{Neo/Neo}$ mouse livers, there were *Pparg* and *Cd36*, encoding the master regulator of lipogenesis and a major receptor for uptake

of free fatty acids, respectively. Quantitative RT-PCR confirmed up-regulation of *Pparg* and *Cd36* in the liver of *Asl*$^{Neo/Neo}$ mice and AAV-mediated delivery of PYGL that rescued histone hypoacetylation associated with nuclear glycogen storage significantly reduced the expression of *Pparg* and *Cd36* (**Figure 29**)

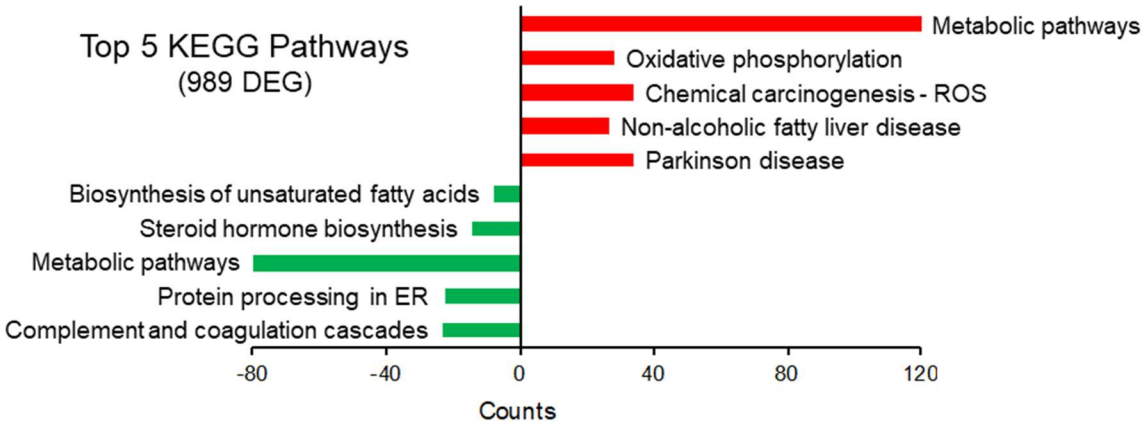

Figure 28: Top 5 over-expressed (in red) and downregulated (in green) of Kyoto Encyclopedia of Genes and Genomes (KEGG) pathways.

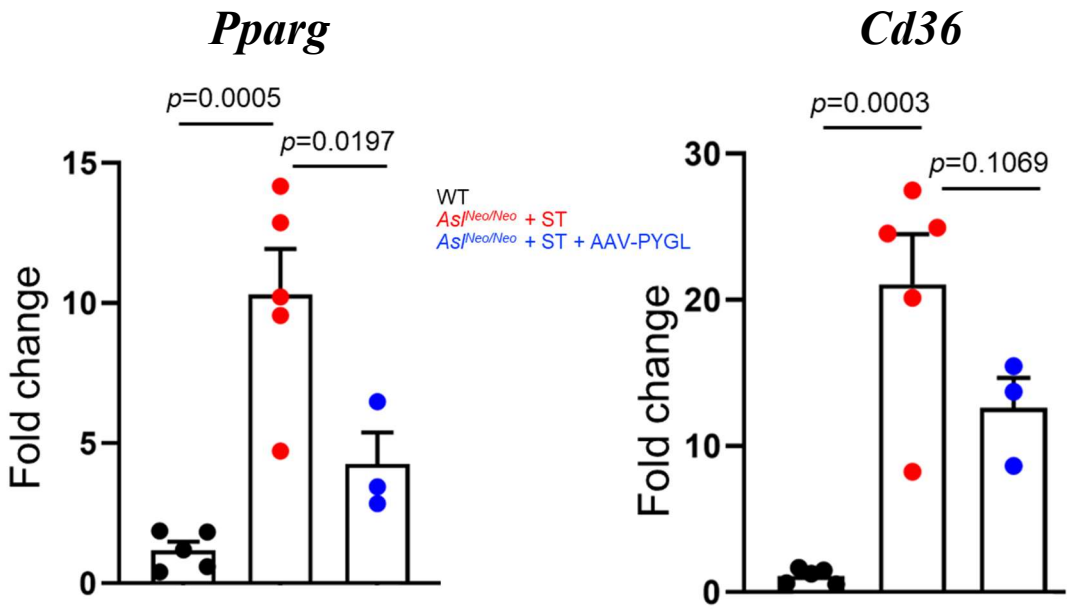

Fig, 29: Real time PCR for *Pparg* and *Cd36* genes on the livers of WT, *Asl*$^{Neo/Neo}$ + ST, and *Asl*$^{Neo/Neo}$ + ST + AAV-PYGL mice. Tukey's One way ANOVA was used for P-value calculations (n=5-3 mice/group).

These findings in a rare genetic disorder raised the hypothesis of a more general involvement of nuclear glycogen storage in more common conditions, such as MAFLD. To investigate this

hypothesis, we selected an animal model of early MAFLD, consisting of rats fed with a HFC diet for 2 weeks (De Chiara *et al.*, 2020). Electron microscopy showed nuclear glycogen in the hepatocytes of rats fed with the HFC diet, but not the standard chow (**Figure 30**).

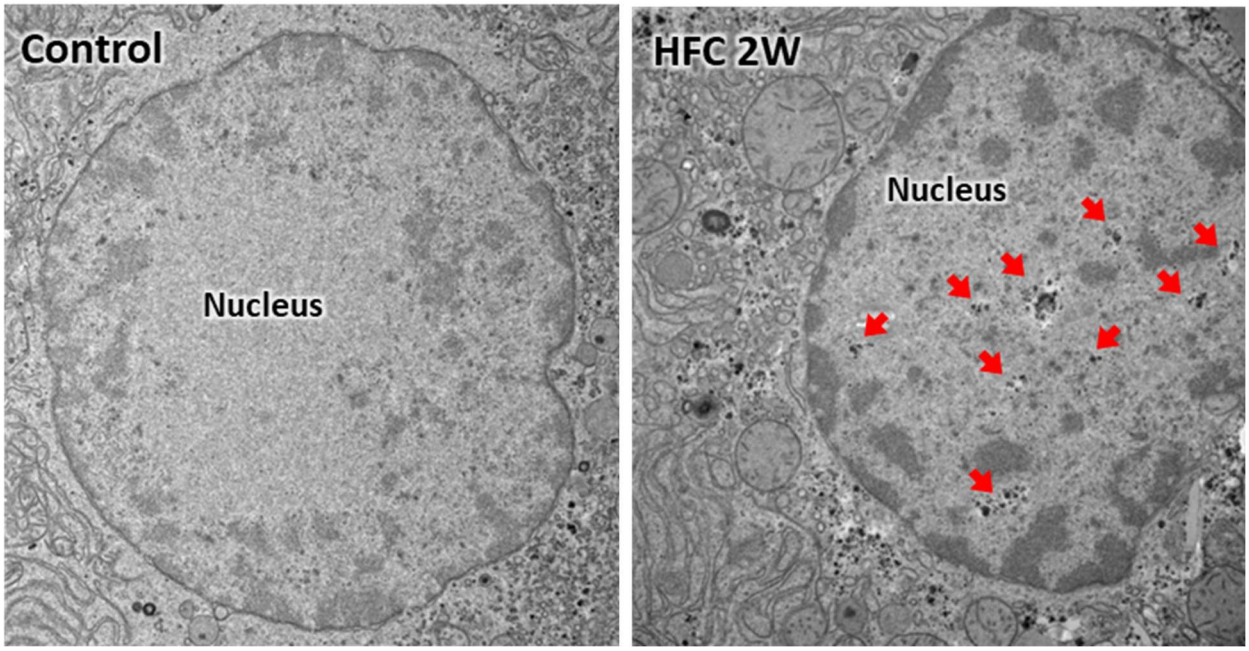

Fig, 30: Electron microscopy of liver samples from a WT rat fed with standard chow (Control) and a WT rat fed for two weeks with high fat, high cholesterol diet (HFC 2W). Red arrows indicate glycogen.

Moreover, consistent with the data in *Asl*$^{Neo/Neo}$ mice, rats fed with HFC showed reduced abundance of PYGL protein in nuclear fractions (**Figure 31A**) and decreased histone acetylation compared to controls (**Figure 31B**).

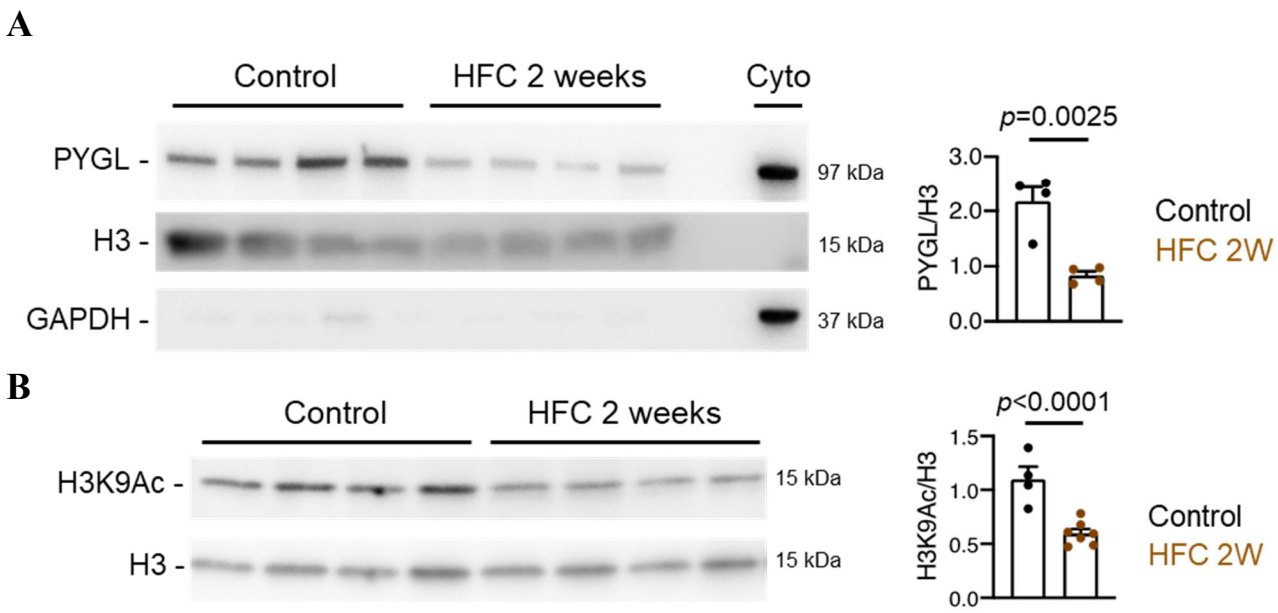

Fig, 31: (A) Western blotting for PYGL on nuclear fractions extracted of livers of WT rats fed with either standard chow (Control) or HFC diet for 2 weeks. A cytosolic fraction (Cyto) is shown as control. Histone H3 was used as loading control and GAPDH as control of the purity of nuclear fractions. Quantification of Western blot bands is shown. **(B)** Western blotting for H3K9Ac on nuclear fractions from livers of control and rats receiving HFC. Histone H3 was used as loading control. Quantification of Western blot bands is shown. Student's t-test was used for p-value calculation (n=4-6 mice/group).

Nitric oxide increases PYGL nuclear translocation

Reduced synthesis of NO is a hallmark of ASA (Nagamani *et al.*, 2012) and it has been previously shown that NO regulates translocation of proteins from the cytosol to the nucleus (Malik *et al.*, 2010). Therefore, we investigated whether supplementation with sodium nitrite, an NO donor, can correct the deficiency of nuclaar PYGL in $Asl^{Neo/Neo}$ mice. Sodium nitrite was indeed found to increase PYGL in nuclear fractions (**Figure 32**) without affecting the total abundance of PYGL (**Figure 33**), supporting a specific role of NO on the nuclear import of the enzyme.

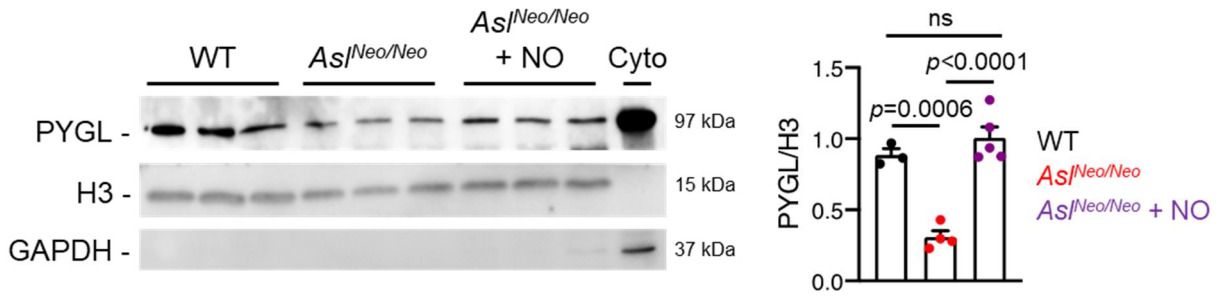

Fig, 32: Western blotting for PYGL on nuclear fractions of livers of WT or *Asl*$^{Neo/Neo}$ mice treated with arginine and sodium benzoate (*Asl*$^{Neo/Neo}$) or with arginine, sodium benzoate and sodium nitrite (*Asl*$^{Neo/Neo}$ + NO); a cytosolic fractions of WT liver is shown. Histone H3 was used as loading control and GAPDH as control of the purity of the nuclear fractions. Western blot quantifications are shown. Tukey's One way ANOVA was used for P-value calculations (n=3-5 mice/group). ns: not statistically significant.

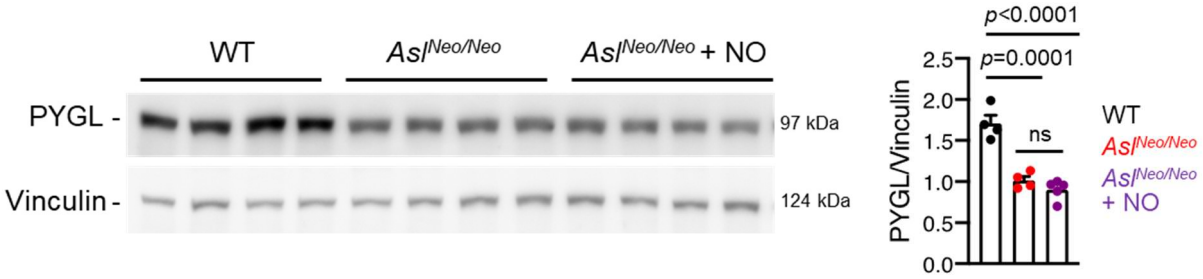

Fig. 33: Western blotting for PYGL on whole liver lysates of WT or *Asl*$^{Neo/Neo}$ mice treated with arginine and sodium benzoate (*Asl*$^{Neo/Neo}$) or with arginine, sodium benzoate and sodium nitrite (*Asl*$^{Neo/Neo}$ + NO). Vinculin was used as loading control. Western blot bands quantifications are shown. Tukey's One way ANOVA was used for p-value calculations (n=4-5 mice/group). ns: not statistically significant.

Consistent with this role, PYGL was previously found to be S-nitrosylated by untargeted mass spectrometry screening (Doulias *et al.*, 2010; Gould *et al.*, 2015) and we confirmed S-nitrosylation of PYGL by the S-nitrosyl biotin switch assay on livers of WT mice (**Figure 34**).

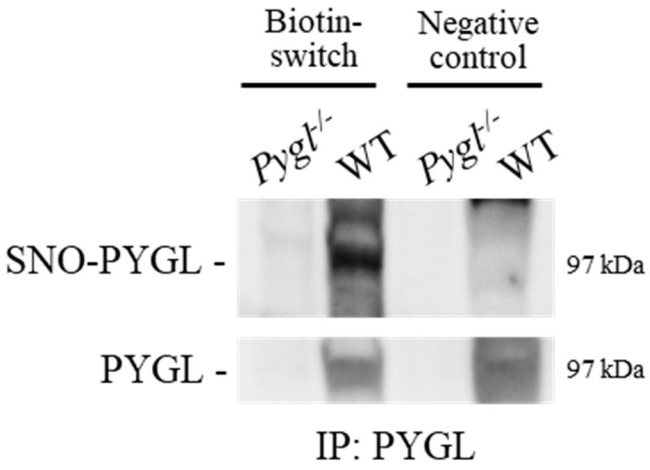

Fig. 34: Immunoblots of liver lysates of WT or *Pygl*$^{-/-}$ mice after immunoprecipitation with anti-PYGL antibody. Biotin-switch assay was performed to convert S-nitrosylation into biotinylation. As negative control, samples were incubated in buffer without reducing reagent. SNO-PYGL, S-nitrosylated PYGL.

DISCUSSSION

ASA is a rare inherited metabolic disorder due to impaired ammonia detoxification (Baruteau *et al.*, 2019). In the livers of both ASA mice and patients glycogen storage has been detected in both cytosol and nucleus (Burrage *et al.*, 2020; Soria *et al.*, 2021). Although nuclear glycogen storage was described in hepatocytes several decades ago, little is still known about its role in physiology and disease states. Nevertheless, recent evidence found that nuclear glycogen storage and reduced glycogenolysis fuel the progression of lung cancer driving epigenetic changes induced by reduced histone acetylation (Sun *et al.*, 2019). In this thesis work, I found that consistent with a previous study (Sun *et al.*, 2019), increased nuclear glycogen results in nuclear metabolic changes including reduced acetyl-CoA-and histone acetylation.

Acetyl-CoA is an essential metabolite required for cell survival and homeostasis and also serves as acyl donor for protein acetylation, thus directly affecting gene expression (Pietrocola *et al.*, 2015). Bulk histone acetylation is highly sensitive to nuclear acetyl-CoA abundance, and the supply of this metabolite for histone acetylation (Sivanand *et al.*, 2018) relies on nuclear synthesis because acetyl-CoA is an unstable metabolite (Bulusu *et al.*, 2017) and has to be produced near to the site of its use. Accordingly, nuclear glycogen catabolism contributes to a compartmentalized pyruvate-derived acetyl-CoA pool (Sun *et al.*, 2019). Beside glycogenolysis, nuclear synthesis of acetyl-CoA is also dependent of other substrates such as citrate and acetate (Sivanand *et al.*, 2018). Consistently, we found a mild reduction of nuclear acetyl-CoA concentration in the livers of $Asl^{Neo/Neo}$ mice. Nuclear glycogen storage is specific for ASA, as it was not observed in other mouse models of UCDs. Moreover, nuclear glycogen was not detected in several mouse models of GSDs, suggesting that nuclear glycogen accumulation is specific for ASA.

Epigenetic alterations play a role in the severity of disease in the liver (Garrido *et al.*, 2022; Wu *et al.*, 2022). In this work, using two independent approaches both resulting in increased histone acetylation, confirmed that epigenetic modifications not involving ASL expression affect the severity of $Asl^{Neo/Neo}$ mice improving their survival. Among the most dysregulated pathways, we found genes involved in lipid metabolism and MAFLD, including the master regulator of lipid metabolism *Pparg,* and the free fatty acid receptor *Cd36*. Delivery of PYGL to the liver of $Asl^{Neo/Neo}$ mice reduced *Pparg* and *Cd36*, supporting the hypothesis changes in *Pparg* and altered lipid homeostasis are dependent on impaired hepatic glycogenolysis. Consistent with the mouse data, alterations of lipid metabolism have been reported also in patients with ASA (Brambilla *et*

al., 2019).

In the last decades rare genetic diseases have been repeatedly instrumental in providing insights and understanding physiology and pathogenic mechanisms of non-genetic disorders with higher prevalence (Hertz *et al.*, 2024). NAFLD, recently renamed as MAFLD, is a frequent liver disorder, with an estimated prevalence of 25% worldwide (Cotter and Rinella, 2020) and has multi-factorial pathogenesis that has not been fully elucidated (Diehl and Day, 2017). Nuclear glycogen storage has been reported in MAFLD patients (Takahashi and Fukusato, 2014) and we confirmed nuclear glycogen accumulation and reduced glycogenolysis and histone acetylation in a diet-induced rat model of MAFLD. Nuclear glycogen storage, appearing as glycogenated nuclei, has been reported in several other liver diseases, including Wilson disease, diabetes, and porphyria cutanea tarda (Fitzpatrick *et al.*, 2014; Lefkowitch and Grossman, 1983; Pronicki, 2017). All these diseases share an increased risk of developing hepatocellular carcinoma, the most common malignant neoplasm of the liver (Campbell *et al.*, 2016; Chen *et al.*, 2012; Ramai *et al.*, 2022). Importantly, hepatocellular carcinoma has been reported in patients with ASA (Baruteau *et al.*, 2017). Impaired nuclear glycogen metabolism and reduced histone acetylation drive progression of lung adenocarcinoma (Sun *et al.*, 2019). For this reason, the role of nuclear glycogen accumulation might be a potential driver for hepatocellular carcinoma. However, further studies are needed to confirm this hypothesis.

Reduced PYGL appears to play an important role in nuclear glycogen storage of ASA mice. Far from being "only" a mediator of vascular smooth muscle relaxation, NO is a key regulator of several processes in the cell. Impaired NO synthesis is a hallmark of ASA (Nagamani *et al.*, 2012). Interestingly, reduced NO synthesis has been found as an early event in the pathogenesis of MAFLD (Nozaki *et al.*, 2015) and mice deficient for NO synthase have glycogen accumulation in the liver (Hocher *et al.*, 2022; Schild *et al.*, 2008). In $Asl^{Neo/Neo}$ mice, I found that increased NO availability increases nuclear PYGL without affecting global protein amount of the enzyme. PYGL undergoes several post-translational modifications regulating its function, including phosphorylation, acetylation and O-GlcNAcylation (Chen *et al.*, 2022; Sprang *et al.*, 1988; Zhang *et al.*, 2012). NO is involved in regulation of protein nuclear translocation through direct S-nitrosylation of cysteine residues (Malik *et al.*, 2010) and PYGL has been reported to be S-nitrosylated (Doulias *et al.*, 2010; Gould *et al.*, 2015). Consistently, we have confirmed S-nitrosylation of PYGL in the liver and we are currently validating this finding by mutagenesis of

the cysteine residues of PYGL. Therefore, the mechanism underlying increased nuclear translocation of PYGL still needs to be clarified. NO-mediated effects on nuclear PYGL might indeed be induced by indirect mechanisms, such as nitrosylation of PYGL interactor partner regulating its nuclear entry. In line with this, previous studies on lung carcinoma cell lines showed that reduced nuclear translocation of PYGB isoform is regulated by protein ubiquitination in the cytoplasm by E3-ubiquitin ligase malin (Sun *et al.*, 2019).

In conclusion, this thesis work provided a working model to explain the role of hepatic nuclear glycogen storage in ASA (**Figure 35**). Our data suggest that reduced NO synthesis, a hallmark of ASL deficiency, is responsible for impaired nuclear translocation of PYGL, resulting in reduced nuclear glycogenolysis and glycogen accumulation. Reduced glycogenolysis is in turn responsible for depletion of nuclear acetyl-CoA and reduced histone acetylation. Global histone hypo-acetylation results in transcriptomic changes that are relevant for the disease severity. These transcriptomic changes include especially genes involved in lipid metabolism and related to pathogenesis of MAFLD. Interestingly, reduced NO synthesis is an important event in the pathogenesis of MAFLD (Fang *et al.*, 2022; Matsumoto *et al.*, 2018). These findings may have implications for development of improved therapies for liver disease in ASA and potentially, other liver disorders with aberrant nuclear glycogen storage.

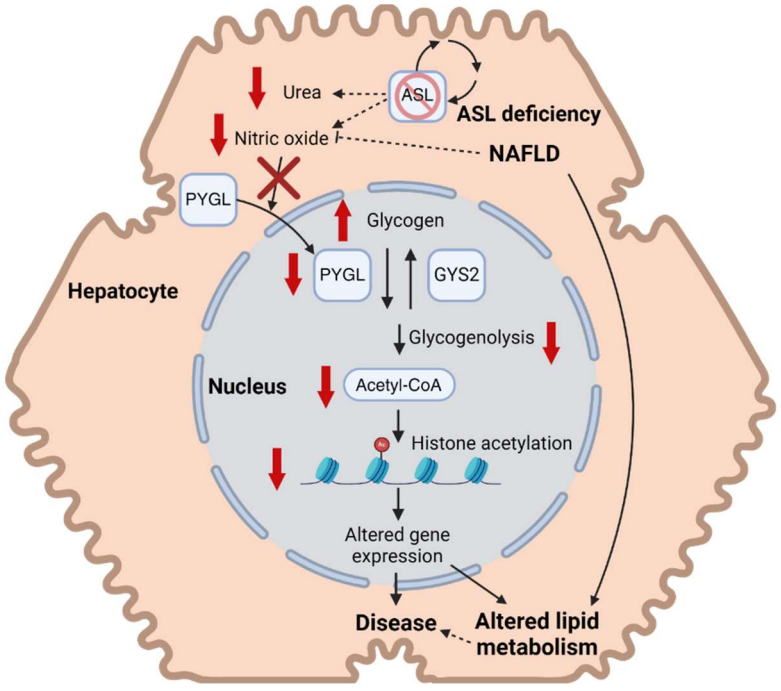

Fig. 35: Proposed working model for the role of nuclear glycogen in the pathogenesis of ASA.

ACKNOWLEDGEMENTS

I am especially thankful to Nicola Brunetti-Pierri for the opportunity to work on this exciting project, for his invaluable mentorship, and for being a constant source of inspiration throughout my research journey. My heartfelt thanks go to Leandro Soria, who taught me a great deal about science and how to work properly, and whose guidance has been invaluable over the past four years. I extend my warm thanks to all members of Nicola Brunetti-Pierri's group—Lucia De Stefano, Claudia Perna, and Iole Boffa—who have always been there to support and help me, and for this, I am truly grateful. Additionally, I thank my former master's thesis student, Paola Arena, and my current master's thesis student, Vincenzo Casertano, for their dedication, assistance, and consistent enthusiasm throughout this journey. I am deeply grateful to Elena Polischchuk for her exceptional electron microscopy analyses, which were essential to this research. I would also like to thank Rossella De Cegli and the TIGEM BiCore for performing the analysis of transcriptomic data, and Nico Mitro for his expertise in nuclear metabolite measurements. I also extend my sincere thanks to Youngmok Lee, Ayelet Erez, Andres Muro, Giuseppe Ronzitti, Karen Louise Thomsen, and Giancarlo Parenti for generously providing samples from their murine and rat disease models. My appreciation goes to Otto Baba for his kind gift of the anti-glycogen antibody.

A special thank you to Edoardo Nusco for being the extraordinary person he is and for his 24/7 support, as well as to all the wonderful people from the TIGEM animal facility for their invaluable support and for all the time spent together in the animal house.

I would also like to thank Professor Daan van Aalten for welcoming me into his lab in Aarhus and for the excellent collaboration we have begun, as well as all members of his group for their support and collegiality.

Finally, I am grateful to Pasquale Piccolo and Margherita Ruoppolo for their insightful suggestions and assistance as members of my PhD committee, and I wish to thank Carlo Dionisi-Vici and Sandro Banfi for their valuable feedback and corrections as thesis evaluators.

These four years have been one of the best experiences of my life, and I am extremely grateful to anyone who contributed to making this possible.

REFERENCES

Abraham S, Furth EE. Receiver operating characteristic analysis of glycogenated nuclei in liver biopsy specimens: quantitative evaluation of their relationship with diabetes and obesity. Hum Pathol. 1994;25(10):1063-1068.

Adeva-Andany MM, González-Lucán M, Donapetry-García C, et al.. Glycogen metabolism in humans. BBA Clin. 2016;5:85-100. Published 2016 Feb 27.

Ah Mew N, Simpson KL, Gropman AL, et al. Urea Cycle Disorders Overview. In: Adam MP, Feldman J, Mirzaa GM, et al. GeneReviews®. Seattle (WA): University of Washington, Seattle; April 29, 2003.

Alderton WK, Cooper CE, Knowles RG. Nitric oxide synthases: structure, function and inhibition. Biochem J. 2001;357(Pt 3):593-615.

Anders S, Pyl PT, Huber W. HTSeq--a Python framework to work with high-throughput sequencing data. Bioinformatics. 2015;31(2):166-169.

Aravinthan A, Verma S, Coleman N, Davies S, Allison M, Alexander Get al.. Vacuolation in hepatocyte nuclei is a marker of senescence. J Clin Pathol. 2012;65(6):557-560.

Ashley SN, Nordin JML, Buza EL, Greig JA, Wilson JMet al. Adeno-associated viral gene therapy corrects a mouse model of argininosuccinic aciduria. Mol Genet Metab. 2018;125(3):241-250.

Audano M, Pedretti S, Ligorio S, Giavarini F, Caruso D, Mitro Net al.. Investigating metabolism by mass spectrometry: From steady state to dynamic view. J Mass Spectrom. 2021;56(1):e4658.

Auricchio A, Hildinger M, O'Connor E, Gao GP, Wilson JMet al.. Isolation of highly infectious and pure adeno-associated virus type 2 vectors with a single-step gravity-flow column. Hum Gene Ther. 2001;12(1):71-76.

Baba O. Kokubyo Gakkai Zasshi. 1993;60(2):264-287.

Bali DS, Goldstein JL, Fredrickson K, et al. Variability of disease spectrum in children with liver phosphorylase kinase deficiency caused by mutations in the PHKG2 gene. Mol Genet Metab. 2014;111(3):309-313.

Baruteau J, Diez-Fernandez C, Lerner S, et al. Argininosuccinic aciduria: Recent pathophysiological insights and therapeutic prospects. J Inherit Metab Dis. 2019;42(6):1147-1161.

Baruteau J, Jameson E, Morris AA, et al. Expanding the phenotype in argininosuccinic aciduria: need for new therapies. J Inherit Metab Dis. 2017;40(3):357-368.

Baskaran S, Roach PJ, DePaoli-Roach AA, Hurley TD. Structural basis for glucose-6-phosphate

activation of glycogen synthase. Proc Natl Acad Sci U S A. 2010;107(41):17563-17568.
Bigot A, Tchan MC, Thoreau B, et al. Liver involvement in urea cycle disorders: a review of the literature. J Inherit Metab Dis. 2017;40(6):757-769.
Boukouris AE, Zervopoulos SD, Michelakis ED. Metabolic Enzymes Moonlighting in the Nucleus: Metabolic Regulation of Gene Transcription. Trends Biochem Sci. 2016;41(8):712-730.
Braissant O, McLin VA, Cudalbu C. Ammonia toxicity to the brain. J Inherit Metab Dis. 2013;36(4):595-612.
Brambilla A, Bianchi ML, Cancello R, et al. Resting energy expenditure in argininosuccinic aciduria and in other urea cycle disorders. J Inherit Metab Dis. 2019;42(6):1105-1117.
Brunt EM. Nonalcoholic steatohepatitis: definition and pathology. Semin Liver Dis. 2001;21(1):3-16.
Brusilow SW, Koehler RC, Traystman RJ, Cooper AJ. Astrocyte glutamine synthetase: importance in hyperammonemic syndromes and potential target for therapy. Neurotherapeutics. 2010;7(4):452-470.
Brusilow SW. Urea cycle disorders: clinical paradigm of hyperammonemic encephalopathy. Prog Liver Dis. 1995;13:293-309.
Bulusu V, Tumanov S, Michalopoulou E, et al. Acetate Recapturing by Nuclear Acetyl-CoA Synthetase 2 Prevents Loss of Histone Acetylation during Oxygen and Serum Limitation. Cell Rep. 2017;18(3):647-658.
Burrage LC, Madan S, Li X, et al. Chronic liver disease and impaired hepatic glycogen metabolism in argininosuccinate lyase deficiency. JCI Insight. 2020;5(4):e132342.
Burwinkel B, Bakker HD, Herschkovitz E, et al. Mutations in the liver glycogen phosphorylase gene (PYGL) underlying glycogenosis type VI. Am J Hum Genet. 1998;62(4):785-791.
Calder PC, Geddes R. Glycogen of high molecular weight from mammalian muscle. Carbohydr Res. 1985;135(2):249-256.
Campbell PT, Newton CC, Freedman ND, et al. Body Mass Index, Waist Circumference, Diabetes, and Risk of Liver Cancer for U.S. Adults. Cancer Res. 2016;76(20):6076-6083.
Chachlaki K, Prevot V. Nitric oxide signalling in the brain and its control of bodily functions. Br J Pharmacol. 2020;177(24):5437-5458.
Chen Y, Wang X, Wang J, et al. Excess body weight and the risk of primary liver cancer: an updated meta-analysis of prospective studies. Eur J Cancer. 2012;48(14):2137-2145.

Chen YF, Zhu JJ, Li J, Ye XS. O-GlcNAcylation increases PYGL activity by promoting phosphorylation. Glycobiology. 2022;32(2):101-109.

Coomes MW, Amino acid metabolism. IN: Devlin TM, editor. Textbook of biochemistry with clinical correlations. Hoboken, NJ: Wiley-Liss; 2006. P.743-82

Cotter TG, Rinella M. Nonalcoholic Fatty Liver Disease 2020: The State of the Disease. Gastroenterology. 2020;158(7):1851-1864.

Coulter DL, Beals TF, Allen RJ. Neurotrichosis: hair-shaft abnormalities associated with neurological diseases. Dev Med Child Neurol. 1982;24(5):634-644.

Crosas E, Sumoy L, González E, et al. The yeast ζ-crystallin/NADPH:quinone oxidoreductase (Zta1p) is under nutritional control by the target of rapamycin pathway and is involved in the regulation of argininosuccinate lyase mRNA half-life. FEBS J. 2015;282(10):1953-1964.

Cunningham RP, Porat-Shliom N. Liver Zonation - Revisiting Old Questions With New Technologies. Front Physiol. 2021;12:732929.

Curtino JA, Aon MA. From the seminal discovery of proteoglycogen and glycogenin to emerging knowledge and research on glycogen biology. Biochem J. 2019;476(21):3109-3124.

D'Alessio AM, Boffa I, De Stefano L, et al. Liver gene transfer for metabolite detoxification in inherited metabolic diseases. FEBS Lett. 2024;598(19):2372-2384.

De Chiara F, Thomsen KL, Habtesion A, et al. Ammonia Scavenging Prevents Progression of Fibrosis in Experimental Nonalcoholic Fatty Liver Disease. Hepatology. 2020;71(3):874-892.

Diehl AM, Day C. Cause, Pathogenesis, and Treatment of Nonalcoholic Steatohepatitis. N Engl J Med. 2017;377(21):2063-2072.

Doria M, Ferrara A, Auricchio A. AAV2/8 vectors purified from culture medium with a simple and rapid protocol transduce murine liver, muscle, and retina efficiently. Hum Gene Ther Methods. 2013;24(6):392-398.

Doulias PT, Greene JL, Greco TM, et al. Structural profiling of endogenous S-nitrosocysteine residues reveals unique features that accommodate diverse mechanisms for protein S-nitrosylation. Proc Natl Acad Sci U S A. 2010;107(39):16958-16963.

Doulias PT, Tenopoulou M, Greene JL, et al.. Nitric oxide regulates mitochondrial fatty acid metabolism through reversible protein S-nitrosylation. Sci Signal. 2013;6(256):rs1.

Ehrlich. Ueber das Vorkommen von Glycogen in diabetischen und normalen Organismus. Zeitschr. f. klin. Med.. 1883, Bd. vi. p. 33.

Elkhateeb N, Olivieri G, Siri B, et al. Natural history of epilepsy in argininosuccinic aciduria provides new insights into pathophysiology: A retrospective international study. Epilepsia. 2023;64(6):1612-1626.

ENCODE Project Consortium. An integrated encyclopedia of DNA elements in the human genome. Nature. 2012;489(7414):57-74.

Ercan-Fang N, Gannon MC, Rath VL, Treadway JL, Taylor MR, Nuttall FQet al.. Integrated effects of multiple modulators on human liver glycogen phosphorylase a. Am J Physiol Endocrinol Metab. 2002;283(1):E29-E37.

Erez A, Nagamani SC, Shchelochkov OA, et al. Requirement of argininosuccinate lyase for systemic nitric oxide production. Nat Med. 2011;17(12):1619-1626.

Eslam M, Sanyal AJ, George J; International Consensus Panel. MAFLD: A Consensus-Driven Proposed Nomenclature for Metabolic Associated Fatty Liver Disease. Gastroenterology. 2020a;158(7):1999-2014.e1.

Eslam M, Newsome PN, Sarin SK, et al. A new definition for metabolic dysfunction-associated fatty liver disease: An international expert consensus statement. J Hepatol. 2020b;73(1):202-209.

Fang ZQ, Ruan B, Liu JJ, et al. Notch-triggered maladaptation of liver sinusoidal endothelium aggravates nonalcoholic steatohepatitis through endothelial nitric oxide synthase. Hepatology. 2022;76(3):742-758.

Fitzpatrick E, Cotoi C, Quaglia A, et al.. Hepatopathy of Mauriac syndrome: a retrospective review from a tertiary liver centre. Arch Dis Child. 2014;99(4):354-357.

Garrido A, Kim E, Teijeiro A, et al. Histone acetylation of bile acid transporter genes plays a critical role in cirrhosis. J Hepatol. 2022;76(4):850-861.

Gould N, Doulias PT, Tenopoulou M, et al. Regulation of protein function and signaling by reversible cysteine S-nitrosylation. J Biol Chem. 2013;288(37):26473-26479.

Gould NS, Evans P, Martínez-Acedo P, et al. Site-Specific Proteomic Mapping Identifies Selectively Modified Regulatory Cysteine Residues in Functionally Distinct Protein Networks. Chem Biol. 2015;22(7):965-975.

Grioni D, Furlan F, Corbetta C, et al. Epilepsy and argininosuccinic aciduria. Neuropediatrics. 2011;42(3):97-103.

Griswold-Prenner I, Kashyap AK, et al. Unveiling the human nitroproteome: Protein tyrosine nitration in cell signaling and cancer. J Biol Chem. 2023;299(8):105038.

Gümüş E, Özen H. Glycogen storage diseases: An update. World J Gastroenterol. 2023;29(25):3932-3963.

Gurung S, Timmermand OV, Perocheau D, et al. mRNA therapy corrects defective glutathione metabolism and restores ureagenesis in preclinical argininosuccinic aciduria. Sci Transl Med. 2024;16(729):eadh1334.

Häberle J, Burlina A, Chakrapani A, et al. Suggested guidelines for the diagnosis and management of urea cycle disorders: First revision. J Inherit Metab Dis. 2019;42(6):1192-1230.

Häberle J. Clinical and biochemical aspects of primary and secondary hyperammonemic disorders. Arch Biochem Biophys. 2013;536(2):101-108.

Hannah WB, Derks TGJ, Drumm ML, Grünert SC, Kishnani PS, Vissing Jet al.. Glycogen storage diseases. Nat Rev Dis Primers. 2023;9(1):46.

Haussinger D. Nitrogen metabolism in liver: structural and functional organization and physiological relevance. Biochem J. 1990. 267: 281-290.

He Y, Yu Z, Chen S. Alpha-Synuclein Nitration and Its Implications in Parkinson's Disease. ACS Chem Neurosci. 2019;10(2):777-782.

Hertz E, Chen Y, Sidransky E. Gaucher disease provides a unique window into Parkinson disease pathogenesis. Nat Rev Neurol. 2024;20(9):526-540.

Hocher B, Lu YP, Reichetzeder C, et al. Paternal eNOS deficiency in mice affects glucose homeostasis and liver glycogen in male offspring without inheritance of eNOS deficiency itself. Diabetologia. 2022;65(7):1222-1236.

Jiang M, Zhao XM, Jiang ZS, et al. Protein tyrosine nitration in atherosclerotic endothelial dysfunction. Clin Chim Acta. 2022;529:34-41.

Keppens S, Vandekerckhove A, Moshage H, et al. Regulation of glycogen phosphorylase activity in isolated human hepatocytes. Hepatology. 1993;17(4):610-614.

Keshet R, Lee JS, Adler L, et al. Targeting purine synthesis in ASS1-expressing tumors enhances the response to immune checkpoint inhibitors. Nat Cancer. 2020;1(9):894-908.

Kho J, Polak U, Jiang MM, et al. Argininosuccinate lyase deficiency causes blood-brain barrier disruption via nitric oxide-mediated dysregulation of claudin expression. JCI Insight. 2023;8(17):e168475.

Kölker S, Garcia-Cazorla A, Valayannopoulos V, et al. The phenotypic spectrum of organic acidurias and urea cycle disorders. Part 1: the initial presentation [published correction appears in

J Inherit Metab Dis. 2015 Nov;38(6):1155-6.]. J Inherit Metab Dis. 2015;38(6):1041-1057.
Koutsifeli P, Varma U, Daniels LJ, et al. Glycogen-autophagy: Molecular machinery and cellular mechanisms of glycophagy. J Biol Chem. 2022;298(7):102093.
Kumari R, Kumar R, Dey AK, et al. S-Nitrosylation of OTUB1 Alters Its Stability and Ubc13 Binding. ACS Chem Neurosci. 2022;13(10):1517-1525.
Kuypers, M., Marchant, H. & Kartal, B. The microbial nitrogen-cycling network. Nat Rev Microbiol 16, 263–276 (2018).
Layton C., Bancroft J.D. Carbohydrates. In: Suvarna S.K., Layton C., Bancroft J.D., editors. Bancroft's Theory and Practice of Histological Techniques. 8th ed. Elsevier; Amsterdam, The Netherlands: 2019. pp. 176–197.
Lefkowitch JH, Grossman ME. Hepatic pathology in porphyria cutanea tarda. Liver. 1983;3(1):19-29.
Lisjak M, Iaconcig A, Guarnaccia C, et al. Lethality rescue and long-term amelioration of a citrullinemia type I mouse model by neonatal gene-targeting combined to SaCRISPR-Cas9. Mol Ther Methods Clin Dev. 2023;31:101103.
Liu X, Gilbert RG. Normal and abnormal glycogen structure - A review. Carbohydr Polym. 2024;338:122195.
Malfatti E, Nilsson J, Hedberg-Oldfors C, et al. A new muscle glycogen storage disease associated with glycogenin-1 deficiency. Ann Neurol. 2014;76(6):891-898.
Malik M, Shukla A, Amin P, et al. S-nitrosylation regulates nuclear translocation of chloride intracellular channel protein CLIC4. J Biol Chem. 2010;285(31):23818-23828.
Marble M, McGoey RR, Mannick E, et al. Living related liver transplant in a patient with argininosuccinic aciduria and cirrhosis: metabolic follow-up [published correction appears in J Pediatr Gastroenterol Nutr. 2008 Jul;47(1):113.]. J Pediatr Gastroenterol Nutr. 2008;46(4):453-456.
Marr L, Biswas D, Daly LA, et al. Mechanism of glycogen synthase inactivation and interaction with glycogenin. Nat Commun. 2022;13(1):3372.
Matsumoto M, Zhang J, Zhang X, et al. The NOX1 isoform of NADPH oxidase is involved in dysfunction of liver sinusoids in nonalcoholic fatty liver disease. Free Radic Biol Med. 2018;115:412-420.
Matsumoto, S., Häberle, J., Kido, J. et al. Urea cycle disorders—update. J Hum Genet 64, 833–

847 (2019).
McCorvie TJ, Loria PM, Tu M, et al. Molecular basis for the regulation of human glycogen synthase by phosphorylation and glucose-6-phosphate. Nat Struct Mol Biol. 2022;29(7):628-638.
Mori T, Nagai K, Mori M, et al. Progressive liver fibrosis in late-onset argininosuccinate lyase deficiency. Pediatr Dev Pathol. 2002;5(6):597-601.
Musumeci O, Pugliese A, Oteri R, et al. A new phenotype of muscle glycogen synthase deficiency (GSD0B) characterized by an adult-onset myopathy without cardiomyopathy. Neuromuscul Disord. 2022;32(7):582-589.
Mutel E, Abdul-Wahed A, Ramamonjisoa N, et al. Targeted deletion of liver glucose-6 phosphatase mimics glycogen storage disease type 1a including development of multiple adenomas. J Hepatol. 2011;54(3):529-537.
Nagamani SC, Campeau PM, Shchelochkov OA, et al. Nitric-oxide supplementation for treatment of long-term complications in argininosuccinic aciduria. Am J Hum Genet. 2012;90(5):836-846.
Nagamani SCS, Erez A, Lee B. Argininosuccinate Lyase Deficiency. In: Adam MP, Feldman J, Mirzaa GM, Pagon RA, Wallace SE, Amemiya A, eds. GeneReviews®. Seattle (WA): University of Washington, Seattle; February 3, 2011.
Newnham T, Hardikar W, Allen K, et al. Liver transplantation for argininosuccinic aciduria: clinical, biochemical, and metabolic outcome. Liver Transpl. 2008;14(1):41-45.
Nozaki Y, Fujita K, Wada K, et al. Deficiency of eNOS exacerbates early-stage NAFLD pathogenesis by changing the fat distribution. BMC Gastroenterol. 2015;15:177.
Nuttall FQ, Gannon MC, Bai G, Lee EY. Primary structure of human liver glycogen synthase deduced by cDNA cloning. Arch Biochem Biophys. 1994;311(2):443-449.
O'Brien WE, McInnes R, Kalumuck K, Adcock M. Cloning and sequence analysis of cDNA for human argininosuccinate lyase. Proc Natl Acad Sci U S A. 1986;83(19):7211-7215.
Ozen H. Glycogen storage diseases: new perspectives. World J Gastroenterol. 2007;13(18):2541-2553.
Palm DC, Rohwer JM, Hofmeyr JH. Regulation of glycogen synthase from mammalian skeletal muscle--a unifying view of allosteric and covalent regulation. FEBS J. 2013;280(1):2-27.
Perito ER, Rhee S, Roberts JP, Rosenthal P. Pediatric liver transplantation for urea cycle disorders and organic acidemias: United Network for Organ Sharing data for 2002-2012. Liver Transpl. 2014;20(1):89-99.

Pietrocola F, Galluzzi L, Bravo-San Pedro JM, et al. Acetyl coenzyme A: a central metabolite and second messenger. Cell Metab. 2015;21(6):805-821.

Pinto HC, Baptista A, Camilo ME, et al. Nonalcoholic steatohepatitis. Clinicopathological comparison with alcoholic hepatitis in ambulatory and hospitalized patients. Dig Dis Sci. 1996;41(1):172-179.

Preiss J, Walsh DA. The comparative biochemistry of glycogen and starch. In: Ginsburg V, Robbins P, editors. Biology of Carbohydrates. John Wiley and Sons; New York: 1981. pp. 199–314.

Pronicki M. Wilson disease - liver pathology. Handb Clin Neurol. 2017;142:71-75.

Ramai D, Deliwala SS, Chandan S, et al. Risk of Hepatocellular Carcinoma in Patients with Porphyria: A Systematic Review. Cancers (Basel). 2022;14(12):2947.

Roach PJ, Depaoli-Roach AA, Hurley TD, Tagliabracci VS. Glycogen and its metabolism: some new developments and old themes. Biochem J. 2012;441(3):763-787.

Roach PJ. Glycogen and its metabolism. Curr Mol Med. 2002;2(2):101-120.

Rocha BS, Gago B, Barbosa RM, et al. Pepsin is nitrated in the rat stomach, acquiring antiulcerogenic activity: a novel interaction between dietary nitrate and gut proteins. Free Radic Biol Med. 2013;58:26-34.

Rybicka KK. Glycosomes--the organelles of glycogen metabolism. Tissue Cell. 1996;28(3):253-265.

Sampaleanu LM, Yu B, Howell PL. Mutational analysis of duck delta 2 crystallin and the structure of an inactive mutant with bound substrate provide insight into the enzymatic mechanism of argininosuccinate lyase. J Biol Chem. 2002;277(6):4166-4175.

Schild L, Dombrowski F, Lendeckel U, et al. Impairment of endothelial nitric oxide synthase causes abnormal fat and glycogen deposition in liver. Biochim Biophys Acta. 2008;1782(3):180-187.

Schwertheim S, Kälsch J, Jastrow H, et al. Characterization of two types of intranuclear hepatocellular inclusions in NAFLD. Sci Rep. 2020;10(1):16533.

Semrau MS, Giachin G, Covaceuszach S, et al. Molecular architecture of the glycogen- committed PP1/PTG holoenzyme. Nat Commun. 2022;13(1):6199.

Shvedunova M, Akhtar A. Modulation of cellular processes by histone and non-histone protein acetylation. Nat Rev Mol Cell Biol. 2022;23(5):329-349.

Sivanand S, Viney I, Wellen KE. Spatiotemporal Control of Acetyl-CoA Metabolism in Chromatin Regulation. Trends Biochem Sci. 2018;43(1):61-74.

Soon GST, Torbenson M. The Liver and Glycogen: In Sickness and in Health. Int J Mol Sci. 2023;24(7):6133.

Soria LR, Gurung S, De Sabbata G, et al. Beclin-1-mediated activation of autophagy improves proximal and distal urea cycle disorders. EMBO Mol Med. 2021;13(2):e13158.

Sprang SR, Acharya KR, Goldsmith EJ, et al. Structural changes in glycogen phosphorylase induced by phosphorylation. Nature. 1988;336(6196):215-221.

Stein LY, Klotz MG. The nitrogen cycle. Curr Biol. 2016;26(3):R94-R98.

Summar ML, Koelker S, Freedenberg D, et al. The incidence of urea cycle disorders. Mol Genet Metab. 2013;110(1-2):179-180.

Summar ML, Mew NA. Inborn Errors of Metabolism with Hyperammonemia: Urea Cycle Defects and Related Disorders. Pediatr Clin North Am. 2018;65(2):231-246.

Sun RC, Dukhande VV, Zhou Z, et al. Nuclear Glycogenolysis Modulates Histone Acetylation in Human Non-Small Cell Lung Cancers. Cell Metab. 2019;30(5):903-916.e7.

Takahashi Y, Fukusato T. Histopathology of nonalcoholic fatty liver disease/nonalcoholic steatohepatitis. World J Gastroenterol. 2014;20(42):15539-15548.

Tarallo A, Damiano C, Strollo S, et al. Correction of oxidative stress enhances enzyme replacement therapy in Pompe disease. EMBO Mol Med. 2021;13(11):e14434.

Thomsen KL, Grønbæk H, Glavind E, et al. Experimental nonalcoholic steatohepatitis compromises ureagenesis, an essential hepatic metabolic function. Am J Physiol Gastrointest Liver Physiol. 2014;307(3):G295-G301.

Turner MA, Simpson A, McInnes RR, Howell PL. Human argininosuccinate lyase: a structural basis for intragenic complementation. Proc Natl Acad Sci U S A. 1997;94(17):9063-9068.

Verdone L, Caserta M, Di Mauro E. Role of histone acetylation in the control of gene expression. Biochem Cell Biol. 2005;83(3):344-353.

Vidal P, Pagliarani S, Colella P, et al. Rescue of GSDIII Phenotype with Gene Transfer Requires Liver- and Muscle-Targeted GDE Expression. Mol Ther. 2018;26(3):890-901.

von Wilamowitz-Moellendorff A, Hunter RW, García-Rocha M, et al. Glucose-6-phosphate-mediated activation of liver glycogen synthase plays a key role in hepatic glycogen synthesis. Diabetes. 2013;62(12):4070-4082.

Waisbren SE, Gropman AL; Members of the Urea Cycle Disorders Consortium (UCDC), Batshaw ML. Improving long term outcomes in urea cycle disorders-report from the Urea Cycle Disorders Consortium. J Inherit Metab Dis. 2016;39(4):573-584.

Wang SB, Venkatraman V, Crowgey EL, et al. Protein S-Nitrosylation Controls Glycogen Synthase Kinase 3β Function Independent of Its Phosphorylation State. Circ Res. 2018;122(11):1517-1531.

Wang Y, Hong F, Yang S. Roles of Nitric Oxide in Brain Ischemia and Reperfusion. Int J Mol Sci. 2022;23(8):4243. Published 2022 Apr 11.

Wilkinson DJ, Smeeton NJ, Watt PW. Ammonia metabolism, the brain and fatigue; revisiting the link. Prog Neurobiol. 2010;91(3):200-219.

Wilson LH, Cho JH, Estrella A, et al. Liver Glycogen Phosphorylase Deficiency Leads to Profibrogenic Phenotype in a Murine Model of Glycogen Storage Disease Type VI. Hepatol Commun. 2019;3(11):1544-1555.

Wilson WA, Skurat AV, Probst B, de Paoli-Roach A, Roach PJ, Rutter Jet al. Control of mammalian glycogen synthase by PAS kinase. Proc Natl Acad Sci U S A. 2005;102(46):16596-16601.

Wu BK, Mei SC, Chen EH, Zheng Y, Pan Det al. YAP induces an oncogenic transcriptional program through TET1-mediated epigenetic remodeling in liver growth and tumorigenesis. Nat Genet. 2022;54(8):1202-1213.

Xiong Y, Soumillon M, Wu J, et al. A Comparison of mRNA Sequencing with Random Primed and 3'-Directed Libraries. Sci Rep. 2017;7(1):14626.

Yaplito-Lee J, Chow CW, Boneh A. Histopathological findings in livers of patients with urea cycle disorders. Mol Genet Metab. 2013;108(3):161-165.

Young FG. Claude Bernard and the discovery of glycogen; a century of retrospect. Br Med J. 1957;1(5033):1431-1437.

Zhang T, Wang S, Lin Y, et al. Acetylation negatively regulates glycogen phosphorylase by recruiting protein phosphatase 1. Cell Metab. 2012;15(1):75-87.